PERFORMANCE ASSESSMENT OF A BINARY CYCLE GEOTHERMAL POWER PLANT

A Thesis Submitted to
the Graduate School of Engineering and Sciences of
İzmir Institute of Technology
in Partial Fulfilment of the Requirements for the Degree of

MASTER OF SCIENCE

in Energy Engineering

by
Murat KARADAŞ

June 2013
İZMİR

We approve the thesis of **Murat KARADAŞ**

Examining Committee Members:

Prof. Dr. H. Murat ÇELİK
Department of City and Regional Planning, İzmir Institute of Technology

Assoc. Prof. Dr. Tahsin BAŞARAN
Department of Architecture, İzmir Institute of Technology

Assist. Prof. Dr. H. Engin DURAN
Department of City and Regional Planning, İzmir Institute of Technology

28 June 2013

Prof. Dr. H. Murat ÇELİK
Supervisor, Department of
City and Regional Planning
İzmir Institute of Technology

Prof. Dr. Gülden GÖKÇEN AKKURT
Co-Supervisor, Department of
Energy Engineering
İzmir Institute of Technology

Prof. Dr. Macit TOKSOY
Co-Supervisor, Department of
Mechanical Engineering,
İzmir Institute of Technology

Prof. Dr. Gülden GÖKÇEN AKKURT
Head of the Department of
Energy Engineering

Prof. Dr. R. Tuğrul SENGER
Dean of the Graduate School of
Engineering and Sciences

ACKNOWLEDGEMENTS

I would like to thank to my supervisor, Prof. Dr. H. Murat ÇELİK and co-supervisors, Prof.Dr. Macit TOKSOY and Prof. Dr. Gülden GÖKÇEN AKKURT for their guidance and for their encouragement during my thesis.

I would like to express special gratitude to Prof. Dr. Macit TOKSOY who was my first advisor before his retirement. If he hadn't given me my thesis subject and plan, this study would have ever occured. I am grateful to him.

My sincere thanks also go to Menderes Geothermal Inc. management for providing plant operation data and the Chairman of the Board of Directors, Muharrem BALAT for supporting this study.

I also would like to thank to my colleagues and Mechanical Operation Department members for their kind assistance during the field tests.

Finally, I want to express my sincere gratitude to my mother Hatice KARADAŞ and my brother Servet KARADAŞ for their endless love and support all the time.

ABSTRACT

PERFORMANCE ASSESSMENT OF A BINARY CYCLE GEOTHERMAL POWER PLANT

An air cooled binary cycle GPP is thermodynamically modeled by using the design data of an actual plant. Effects of design parameters are investigated to plant performance. The modeling binary cycle power plant is produced 6514 kW_e by using 542.65 ton/hour brine, 22.45 ton/hour steam and 33.4% NCGs content of steam at 157.9 °C geothermal resource temperature and 17.1 °C average ambient air conditions. The thermal efficiency of the model plant is found 11.32 %. The performance equations and the theoretical net power correction factors of the plant are created by using the thermodynamic model. According to this model, the net power generation of the plant increases with an increase in brine temperature, and mass flow rates of brine and steam; decreases with an increase of ambient air temperature and NCGs content of the steam.

Furthermore, regression analysis of DORA-1 GPP is conducted using actual plant data to assess the plant performance. The annual multiple linear regression models are developed from 2006 to 2012 to estimate the performance of a geothermal power plant by using three measured dependent variables: the ambient air temperature, the brine flow rate and temperature. These models are tested by using classical assumptions of linear regressions, positive serial autocorrelation is found in all models. Autocorrelations are eliminated by using Orcutt-Cochran method. Although the performance model trends from 2006 to 2008 are found to be close, the performance status of the plant is generally variable from year to year. According to perennial regression models, the plant performance has started to decline with 270 kW_e electricity generation capacity since 2009. The total degradation of the plant performance reached to 760 kW_e capacity by 2012. Additionally, the statistical net power correction factors are calculated using regression model of 2008.

Consequently, the net power correction factors for thermodynamic model and regression analysis are compared with DORA-1's manufacturer, Ormat, correction factors. Although there are some minor differences, all of the net power correction factors have similar trends. The comparison shows that Ormat's correction factors don't exactly express the performance status of the DORA-1 GPP.

ÖZET

ÇİFT AKIŞKANLI BİR JEOTERMAL GÜÇ SANTRALININ PERFORMANS DEĞERLENDİRMESİ

Gerçek bir jeotermal elektrik santralının tasarım parametreleri kullanılarak hava soğutmalı çift akışkanlı bir jeotermal elektrik santralı tasarlanmış ve tasarım parametrelerinin teorik santral performansına etkisi incelenmiştir. Teorik santral 157.9 ˚C'deki 542.65 ton/saat jeotermal akışkan, 22.45 ton/saat buhar ve %33.4 oranda yoğuşmayan gazlar ile 17.1 ˚C dış ortam sıcaklığında 6514 kW_e elektrik üretebilmektedir. Teorik santral modelinin ısıl verimi %11.32 bulunmuştur. Termodinamik model kullanılarak santralın performans denklemleri ve net güç üretimi düzeltme faktörleri bulunmuştur. Bu modele göre net güç üretimi jeotermal akışkan sıcaklığı, debisi ve buhar debisinin artması ile artmakta; dış hava sıcaklığı ve yoğuşmayan gazlar oranının artması ile düşmektedir.

Ayrıca, santral performansının durumunu değerlendirebilmek için DORA-1 jeotermal elektrik santralının gerçek verileri kullanılarak regresyon analizi yapılmıştır. Dış hava sıcaklığı, jeotermal akışkan debisi ve sıcaklığı gibi ölçülebilen üç bağımsız değişken kullanılarak, 2006 yılından 2012 yılına kadar yıllık çoklu doğrusal regresyon modelleri geliştirilmiştir. Bu modeller klasik doğrusal regresyonun kabulleri kullanılarak test edilmiş ve tüm modellerin hataları arasında pozitif bağımlılık bulunmuştur. Hatalar arasında pozitif bağımlılık Orcutt-Cochran metodu kullanılarak giderilmiştir. Her ne kadar 2006 yılından 2008 yılına kadarki performans modelleri birbirine yakın olsa da, genel olarak yıldan yıla değişmektedir. Çok yıllık performans modellerine göre 2009 yılından sonra 270 kW_e'lık santral performansında düşüş başlamıştır. Santral performansındaki toplam düşüş 2012 yılı itibariyle 760 kW_e'a ulaşmıştır. Bunlara ek olarak, 2008 yılının regresyon modeli kullanılarak DORA-1 jeotermal elektrik santralının istatistiksel net güç düzeltme faktörleri hesaplanmıştır.

Sonuç olarak termodinamik ve regresyon modelin net güç düzeltme faktörleri DORA-1 jeotermal elektrik santralı için santral üreticisi Ormat tarafından verilen düzeltme faktörleri ile karşılaştırılmıştır. Bazı küçük farklılıklar olmasına karşın, tüm net güç düzeltme faktörleri aynı eğilimi göstermektedir. Net güç düzeltme faktörleri karşılaştırmasından anlaşılmaktadır ki, Ormat'ın düzeltme faktörleri DORA-1 jeotermal elektrik santralı performansını tam olarak ifade etmemektedir.

TABLE OF CONTENTS

LIST OF FIGURES

LIST OF TABLES

LIST OF SYMBOLS

a,b,c,d	Model constants
b_i	Least square estimator
C	Heat capacity, kJ sec^{-1} K^{-1}
c_p	Specific heat, kJ kg^{-1} K^{-1}
Cov	Covariance
d	Durbin-Watson statistics
F	Net power correction factor
h	Enthalpy, kJ kg^{-1}
ṁ	Mass flow rate, kg s^{-1}
$\dot{Q}$	Heat, kW
P	Pressure, bar
R^2	Determination coefficient
s	Entropy, kJ kg^{-1} K^{-1}
S	Error sum of squares
T	Temperature, (°C)
Var	Variance
VIF	Variance Inflaction Vector
$\dot{W}$	Work, kW
X	Independent variable
Y	Dependent variable

Greek Symbols

β	Partial regression coefficient
ε	Effectiveness of heatexchangers
ε_i	Error term
η	Efficiency
σ	Variance

Subscripts

brine	Geothermal fluid

c	Cold
cond	Condenser
gen	Generator
H	High
h	Hot
in	Inlet, inflow
L	Low
min	Minimum
NCG	Non-condensable gases
net	Net power
out	Outlet, outflow
ph	Preheater
pp	Pinch point
s	Isentropic
turb	Turbine
vap	Vaporizer

CHAPTER 1

INTRODUCTION

Population and industrialization in Turkey have been increasing as a developing country, which also has resulted in a tremendous increase in energy demand. According to the information provided by the Ministry of Energy and Natural Resources, electricity consumption of Turkey, which was 229.3 billion kWh in 2011, is expected by 2020 to reach 499 TWh with an annual increase of around 8% according to the higher demand scenario, and 406 TWh with an annual increase of 6.1% according to the lower demand scenario (MENR, 2012).

Currently, over 80% of the energy supply comes from fossil fuels in Turkey. According to Aneke *et al.* (2011), since fossil fuels are exhaustible, there is a need for their conservation. Because of the over dependence on fossil fuels for energy supply, fossil fuels have resulted in the release of large quantity of anthropogenic CO_2 (greenhouse gas) into the environment. They cause environmental pollution and global warming. This associated environmental danger is caused by the burning of fossil fuels and has resulted in a clamor by the world leaders to develop better and more efficient means of meeting the world energy demand with a minimum environmental impact. Recently, there has been a gradual shift from over dependence on fossil fuels to the use of renewable and cleaner energy sources such as wind and geothermal energy.

In Turkey, geothermal energy is a renewable heat energy, which manifests with fluid production temperatures varying from 50 to 287 ^{0}C. It occurs mainly in the form of water and water-steam mixture. Geothermal heat energy has been identified as a good source of power generation. Geothermal power plants (GPPs) differ from thermal power plants in that they have boilers underground and they are less efficient because of low resource temperatures.

In recent years, investments on GPPs have increased with the enactment of regulations and incentives for electricity generation from renewable energy sources. The government provides tax and customs duty exemption for investors who want to generate electricity from renewable energy by the Encouragement of Investments and

Employment Law (TGNA_1, TGNA_2). Currently, the total installed capacity of GPPs in Turkey is 166.35 MW_e, which is expected to increase rapidly by new investments.

Performance of GPPs depends on the thermophysical properties of geothermal reservoir and ambient. Geothermal reservoirs are classified as low, medium and high enthalpy resources, and their temperature ranges are 100–160^{0}C, 160–190^{0}C and over 190^{0}C, respectively (Bronicki, 1995). Although some higher enthalpy wells exist in the Kizildere and Germencik geothermal fields, generally the low and medium enthalpies liquid dominated geothermal resources, which contains high amounts of non-condensable gases (NCGs), exists in Turkey. The presence of NCGs plays an important role in the driving mechanism of the reservoirs because their partial pressure is quite high (Kaplan and Serpen, 2010). Since the most of the fields in Turkey have high content of NCGs, pressure and mass flowrate of geothermal fluids are high and the wells are artesianic.

Energy or thermal efficiency of power plants, which are converted of thermal energy to electricity, is defined as the ratio of provided thermal energy by generated electricity (Kanoglu, 2007). The maximum thermal efficiency of a GPP is limited to the temperature of the geothermal reservoir and ambient conditions. Therefore, the design of a power plant is essentially determined by thermophysical properties of high heat and low heat sources such as temperature, pressure and mass flowrate. In addition, the contents of geothermal fluid, NCGs rate and the other characteristics of the field are vital during the design stage of GPPs.

Performance of a GPP is calculated by deterministic formulations of thermodynamics. However the plant data might be probabilistic because it is possible that inputs could be measured by uncalibrated devices or some parameters may be neglected during the computation. Thus, the performance of GPPs could be estimated by using regression analysis. If the plant designer gives performance correction factors of a GPP, the performance status of the plant can also be calculated.

The aim of the Thesis is:

a. Thermodynamic modeling of a theoretical air cooled binary cycle GPP by using the Engineering Equation Solver software (EES, 2013), according to DORA-1 GPP design parameters,
b. Multiple linear regression analysis of DORA-1GPP performance, using the annual plant data from 2006 to 2012,

c. Defining of the net power correction factors of DORA-1 GPP, which are given by designer: Ormat,
d. Assessment and comparison of theoretical, regression and Ormat performance models.

The geothermal power generation, types of power plants and the status of geothermal power generation in the world and Turkey are introduced in Chapter 2. In Chapter 3, literature survey on thermodynamic modeling of binary GPPs and regression analysis is summarized. The system of DORA-1 GPP is mentioned in Chapter 4. The methodology of thermodynamic, regression and Ormat performance modeling are explained in Chapter 5 and the results of the performance models and their comparisons are presented in Chapter 6. Finally, the conclusions are stated in Chapter 7.

CHAPTER 2

GEOTHERMAL POWER GENERATION

Geothermal energy, which comes from beneath the earth surface with temperatures varying from 50 to 370 ˚C, is a clean, renewable and sustainable natural resource (GEA, 2012). Geothermal sources are used in several areas such as: electricity generation, space heating and cooling, fruit or vegetable drying, aquaculture, swimming, bathing etc. (Figure 2.1).

The first GPP was invented in 1904 by Prince Piero Ginori Conti at the Larderello dry steam geothermal field in Italy. The first GPP in the U.S. was installed in 1962 at the Geysers dry steam field in California (GEO, 2013).

Geothermal exploration studies in Turkey started at the beginning of 1960s in Balçova, İzmir (1963) and in Kizildere, Denizli (1968). Kizildere geothermal field was the first geothermal field to be discovered at high enthalpy. Some medium enthalpy fields such as Seferihisar, Salavatlı and Simav were discovered in 1970s and 1980s. The Kizildere GPP, which was the first GPP of Turkey, was installed in 1984. Kizildere GPP with a 17.4 MW_e electricity generation capacity has been dealt with some problems such as precipitation of calcium carbonate in the wellbores, pipelines and the condenser.

Investment of new GPPs delayed for many years due to the lack of experience in GPP operation and regulatory framework. Many years after the Kizildere experience, DORA-1 GPP was installed in 2006 in Salavatlı, Aydın. Beliefs in the success of the GPP investments increased after the installation of Bereket (Sarayköy, Denizli) and Gurmat (Ömerbeyli, Aydın) GPPs in 2007 and 2009, respectively.

In this chapter, the types of GPPs and the status of geothermal power generation in the World and Turkey will be mentioned.

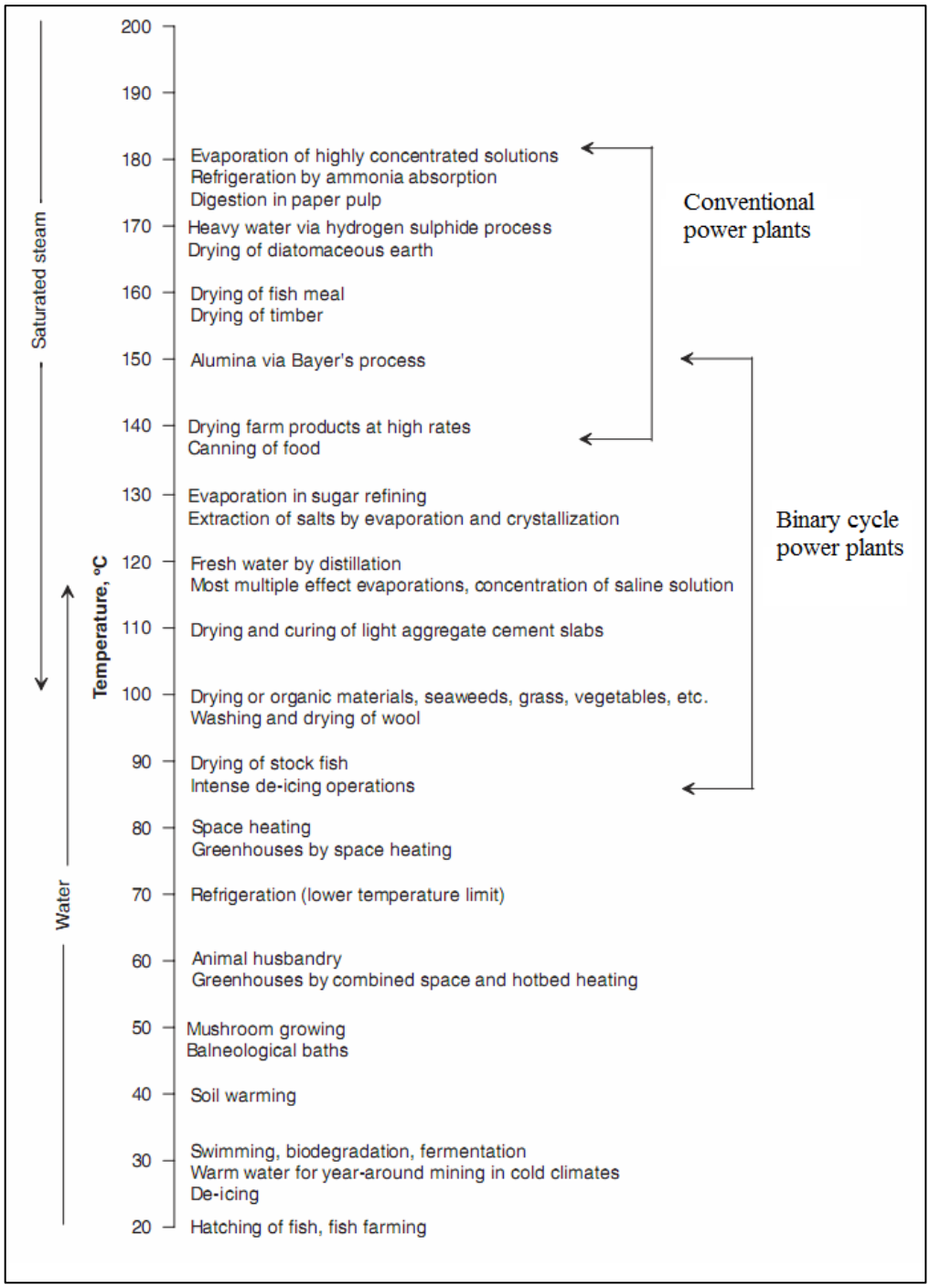

Figure 2.1. Lindal Diagram
(source: Gupta and Roy, 2007).

2.1. Types of Geothermal Power Plants

GPPs are mainly divided into three types: Dry-steam, Flash, and Binary cycle GPPs. In Dry-steam cycle, geothermal steam directly comes from reservoir and it is used to turn turbine blades. Flash and binary cycles are mostly applied to liquid

dominated resources. Since efficiencies of GPPs are lower than the fossil-fuelled power plants, most effective and economical plant type should be selected for geothermal resources (Shokouhmand and Atashkadi, 1997). In the world, some combined cycles such as flash-binary combined cycle and Kalina cycle have been used to increase efficiency and power generation.

2.1.1. Single and Double Flash GPPs

Flash cycle GPPs are generally installed on the high enthalpy geothermal fields. A single flash plant mainly consists of a separator, a turbine-generator unit, a condenser, a cooling tower and a circulation water pump (Figure 2.2). Geothermal fluid, which comes from the wellbore at high pressure, can flash in the reservoir, production well or inlet of the separator (Dipippo, 2005). In this type of plants, the mixture firstly enters a separator, and then two-phase flow is physically separated as steam and liquid phases with a minimum pressure loss in the separator. The separated liquid phase (brine) returns into reinjection line. The steam phase, including NCGs, passes through a ball check valve, enters the turbine at high pressure and drives the blades of turbine to produce electricity. After that steam expands, its pressure drops and flows to the condenser. Steam passes liquid phase in the condenser by using cooling water coming from cooling tower. NCGs are extracted from the condenser by a gas removal system such as compressor or jet ejector (Gokcen et al., 2004). Condensed water is pumped down a reinjection well with separated liquid phase to sustain production.

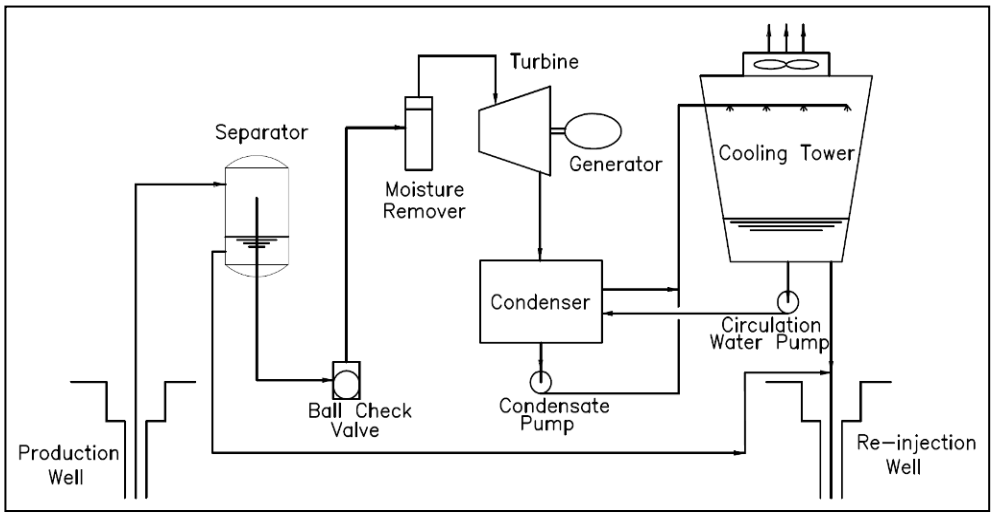

Figure 2.2. Flow diagram of a single flash GPP (adopted from Dipippo, 2005).

Double flash GPPs are different from the single flash GPPs in that they have additional low-pressure separator and turbine. After the first separation, separated liquid phase enters the low-pressure separator, producing low pressure steam. Steam and liquid phases are separated and then steam passes through the low-pressure turbine. It enters the condenser with steam of high-pressure turbine. The rest of the cycle is similar to single flash cycle. A simple schematic diagram of a double flash GPP is shown in Figure 2.3. The double flash plant can produce more power than single flash under the same conditions (Swandaru, 2009).

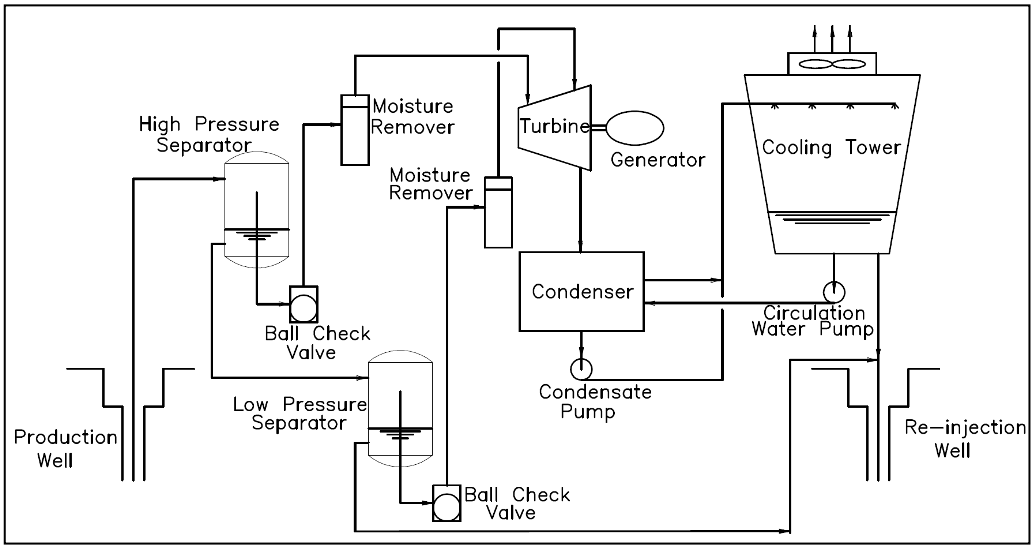

Figure 2.3. Simplified flow diagram of a double flash GPP (adopted from Dipippo, 2005)

2.1.2. Binary Cycle GPP

In binary GPPs, the heat of geothermal fluid is transferred to an organic working fluid in heat exchangers such as preheater and evaporator. Geothermal fluid is used for the heat transfer and passes only in the heat exchangers. The heat of geothermal fluid is transferred to an organic working fluid that has a low boiling point, and then returns to the ground by the reinjection wells to recharge reservoir (Dipippo, 2005). Working fluid becomes saturated or superheated vapor in the heat exchangers. The working fluid then passes through the turbine and electricity is generated. After that, it enters the condenser and is cooled by a cooling fluid until it becomes liquid. Finally, it is pumped to the preheater and the evaporator by a feed pump. The simple schematic of binary cycle power plants is shown in the Figure 2.4.

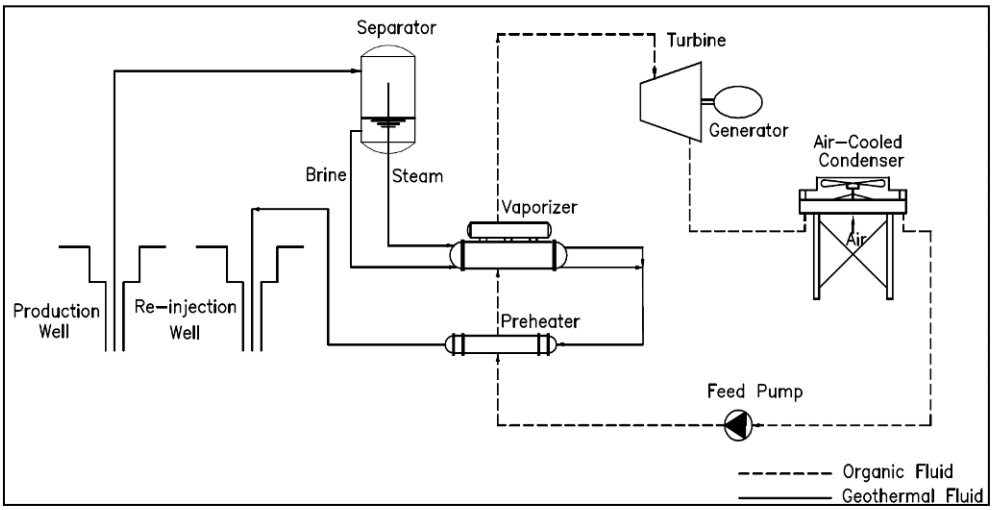

Figure 2.4. Flow diagram of a two phase binary GPP (utilized from Kaplan and Serpen, 2010).

Cooling system is also important in binary plants. If there is an unlimited resource of cooling water in the field, wet cooling system may be used to condensate working fluid by cooling water. Dry air-cooling systems are more suitable for locations with water shortage because in this system, heat of working fluids is rejected directly into air. Another advantage of the air-cooling systems is that there is no emission to the atmosphere. However, parasitic load of cooling fans is excessive because of a need of a large heat transfer surface for condensation. Therefore, the efficiency of the plant significantly decreases with increasing ambient temperatures for air-cooling systems.

In addition, thermo-physical properties of working fluid directly affect the performance of the plant. The main criteria for the selection of the working fluid are evaporation at atmospheric pressures and boiling at low temperatures. The working fluids are generally selected from hydrocarbons such as pentane and isobutane.

Binary systems have more environmental benefits than flash systems because binary GPPs operate in closed circuits and have no loss of working fluid to the environment. Equipment of the binary cycle plants have economically a longer life than the flash type plants because of geothermal fluid does not contact with the turbine or other moving mechanical components of the plant (Franco, 2011).

Currently in Turkey single flash, double flash and binary cycle power plants are in operation. Reservoir characteristics and environmental conditions directly affect the determination of appropriate option of power plant. Since binary cycle is more feasible for low and medium enthalpy geothermal fields because of high concentration of

calcium carbonate and NCG content of geothermal fluids, it is the most common cycle that applied in Turkey (Kaplan and Serpen, 2010). Integrated two level unit (ITLU) types binary cycle power plants, consist of two organic Rankine cycles and CO_2 is separated at the wellhead by a separator passes the heat exchanger at one of the cycles, are the mostly applied in Turkey.

2.1.3. Kalina Cycle GPP

The Kalina cycle is generally used for the maximum utilization of the heat of low temperature geothermal resources. The Kalina GPPs operate as Rankine cycle, but its working fluid is different. Water-ammonia mixture uses as working fluid. A simple Kalina cycle GPP is illustrated in Figure 2.5.

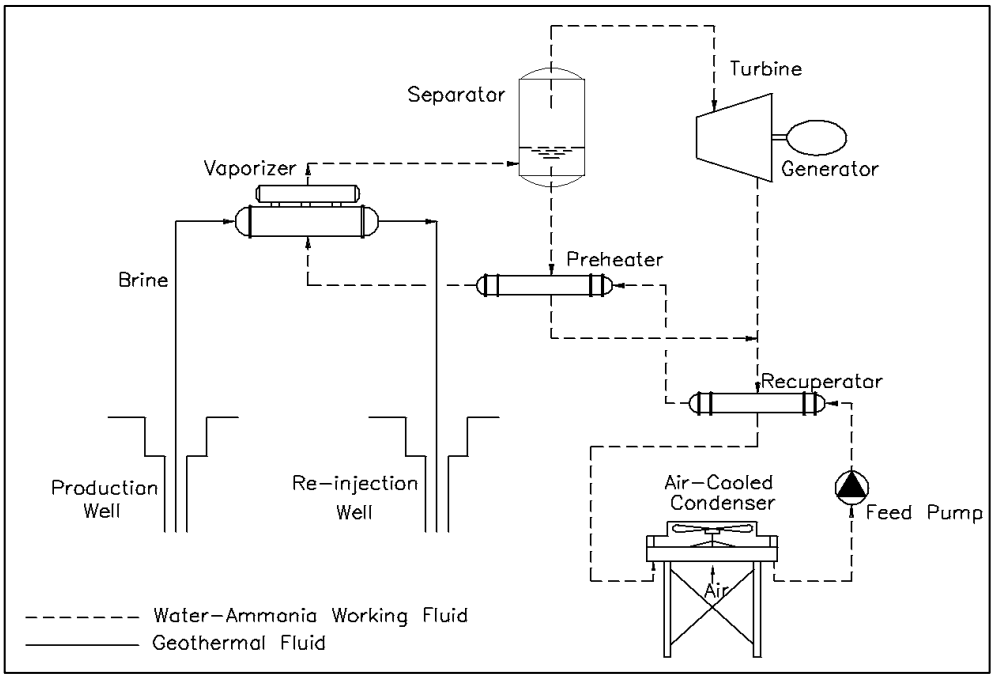

Figure 2.5. Flow diagram of a Kalina cycle GPP.

In the Kalina cycle, geothermal fluid heats the working fluid in the evaporater until saturation temperature and two phases water-ammonia mixture leave the evaporator. Then, it enters the separator. Working fluid is separated as ammonia vapor and saturated ammonia-poor liquid. The saturated ammonia-poor liquid is cooled in the preheater. The ammonia vapor passes through the turbine to generate power and then enters the recuperator with ammonia-poor liquid, cools and condenses in the recuperator and

condenser. After that, it pumps to recuperator, preheater and evaporator for first heating and then boiling (Fu et al., 2013). The Kalina cycle GPPs have a higher thermodynamic efficiency than binary cycle GPPs (Ozcan, 2010).

2.2. Geothermal Power Generation in the World

Power generation from the geothermal sources in the world has increased in recent years (Figure 2.6). GPPs operate at least 24 countries in the world. The total installed capacity of the GPPs reached to 10897.8 MW_e by 2010 and it is expected to reach 18500 MW_e until 2016 (Chamorro et al., 2012).

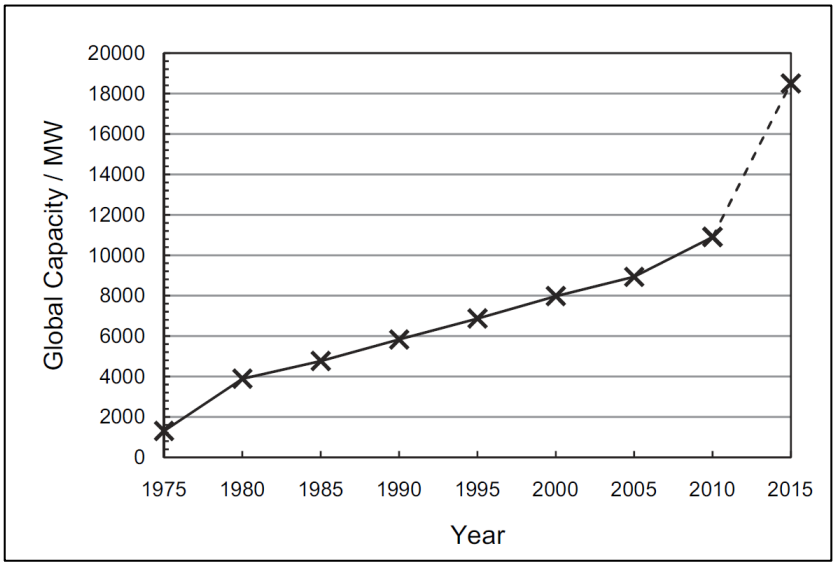

Figure 2.6. Evolution of installed geothermal power capacity from 1975 to 2010 and planned capacity for 2015 (source: Chamorro et al., 2012).

The distribution of the GPP types according to countries is given at Table 2.1.

Table 2.1. World GPP distribution by plant type for 2010 data (source: Chamorro et al., 2012).

Plant type	**Units**	**Installed capacity (MW_e)**	**Average size (MW_e)**	**Percent of total installed capacity (%)**
Dry Steam	61	2822.0	46.3	25.9
Single Flash	145	4551.6	31.4	41.8
Double Flash	64	2182.7	34.1	20.0
Binary/Hybrid	266	1341.5	5.1	12.3
Total	**536**	**10897.8**	**20.3**	**100**

2.3. Present Status of GPPs in Turkey (June, 2013)

The high temperature geothermal fields suitable for conventional electricity generation in Turkey are Denizli-Kizildere (242°C), Aydın-Ömerbeyli (232°C), Aydın-Salavatlı (176°C), Canakkale-Tuzla (174°C), Kutahya-Simav (184°C), Izmir-Seferihisar (153°C) and Manisa-Kavaklıdere (215°C). The other high temperature fields with electricity generation potential are Manisa-Caferbeyli (168°C), Aydın-Yilmazkoy (142°C), Aydın-Umurlu (130°C), Izmir-Dikili (120°C), Izmir-Balcova (125°C).

The operating GPPs of Turkey are listed in Table 2.2.

Table 2.2. GPPs of Turkey as of June 2013 (in operation).

Location	Power plant	Types of GPPs	Startup date	Maximum resource temperature (°C)	Average resource temperature (°C)	Gross power capacity (MW_e)
Denizli						
Kizildere	Zorlu - Kizildere	Single flash	1984	242	217	17.4
Sarayköy	Bereket	Binary cycle	2007	-	145	7.5
Aydın/Sultanhisar						
Salavatlı	Dora-1	Binary Cycle	2006	172	168	7.35
Salavatlı	Dora-2	Binary Cycle	2010	176	175	11.2
Aydın/Germencik						
Ömerbeyli	Gurmat	Double Flash	2009	232	220	47.4
Hıdırbeyli	Irem	Binary Cycle	2011	190	170	20
Bozkoy	Sinem	Binary Cycle	2012	-	-	24
Bozkoy	Deniz	Binary Cycle	2012	-	-	24
Çanakkale						
Tuzla	Tuzla	Binary Cycle	2010	174	160	7.5
Total						**166.35**

According to Table 2.2, 78% of GPPs are binary power plants. The operating temperatures of the all plants range between 145 and 243°C. By June 2013, the total installed capacity of GPPs reached to 166.35 MW_e.

The increase in installed geothermal power capacity of Turkey is exhibited in Figure 2.7 by year. Kizildere GPP, which was the first GPP of Turkey, was installed in 1984. Then, the second GPP was installed 22 years later. Thereafter, investments of power plants have boomed along with the enactment of laws and regulations on power generation from renewables. The GPP (planned and under construction) locations and installed capacities are given in Table 2.3.

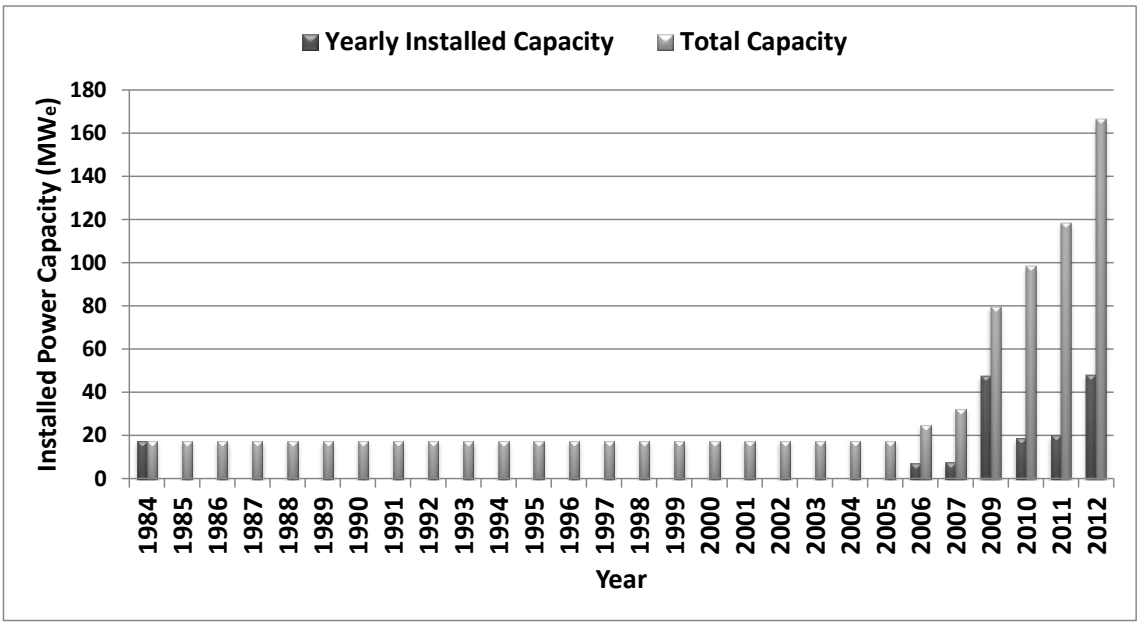

Figure 2.7. Installed GPP capacity of Turkey by year.

Table 2.3. Geothermal power plants as of June 2013 (planned and under construction).

Location	Planned capacity (MW_e)	Maximum temperature (°C)
Manisa		
Merkez	10	-
Alaşehir	20	-
Alaşehir - Piyadeler	24	-
Alaşehir - Erenköy	30	-
Salihli - Caferbeyli	15	168
Denizli		
Sarayköy	3	-
Sarayköy - Seyitler	2.52	-
Sarayköy - Kizildere	86.93	242
Aydın		
Salavatlı: Dora-3	34	180
Salavatlı: Dora-4	17	-
Sultanhisar	9.9	-
Nazilli - Atça	9.5	124
Nazilli - Gedik	20	-
Köşk - Umurlu	5	131
Germencik – Gümüşköy	13.2	-
Germencik-Ömerbeyli	162.5	-
Merkez	24	-
Kuyucak – Pamukören	30	-
Çanakkale		
Ayvacık	3	-
Total	**519.55**	

By the end of 2013, Salavatlı-Dora-3 unit1, Germencik-Gümüşköy and Sarayköy-Kizildere GPP projects are expected to be in operation and the total installed capacity of Turkey is expected to be 285.28 MW_e. Also installed capacity of all geothermal plants is expected to reach up 500 MW_e with additional GPPs by the year of 2015 (EMRA, 2013).

CHAPTER 3

LITERATURE SURVEY

GPPs are designed to provide a rated power output according to specific geothermal resource properties and ambient conditions (Mines, 2002). Geothermal resource temperature is generally constant while the air temperature changes throughout the year. Therefore, seasonal changes in the ambient air temperature directly affect the thermal efficiency of a GPP. The maximum thermal efficiency of a thermal energy source is limited to the Carnot efficiency (Kanoglu, 2007). On the other hand, the Carnot efficiency is not valid as a reference for low temperature geothermal sources (Valdimarsson, 2003). Valdimarsson (2003) introduces power generation from geothermal heat and ideal cycles. He analyzed the performance of plants when the thermophysical properties of geothermal source and the heat sink changed.

In the literature, there are a lot of optimization studies in which actual binary GPPs data is used. Ghasemi et al. (2013) simulated an air cooled binary GPP by ASPEN Plus and optimized the component of the plant for maximum net power output. Hettiarachchi et al. (2006) conducted on optimization study which focused on the ratio of the total heat exchanger area to net power output. Temperatures of evaporation and condensation and velocities of geothermal and cooling water were the variables of the study. The optimum cycle performance was evaluated and compared with various working fluid. Guo et al. (2011), conducted an optimization study for the ORC-based power generation system. Net power output per unit mass flow rate of hot source, the ratio of total heat transfer area to net power output, and electricity generation cost were the screening criteria of the study.

In thermodynamic performance analysis of GPPs, exergy analysis based on the second law of the thermodynamics has proven to be a powerful tool (Kanoglu and Bolatturk, 2008). In the literature, there are many studies which have focused on energy and exergy analysis of binary GPPs. Kanoglu (2002) conducted an exergy analysis of a binary GPP in which actual plant data was used to evaluate the plant performance and pinpoint sites of primary exergy destruction. The results showed that the greatest exergy destruction occurred in the condenser which accounts for 22.6 %. Coskun et al. (2011)

performed thermodynamic analysis and performance investigation of Tuzla binary GPP. In this study, eight energetic-exergetic performance parameters were also introduced. They found that the largest energy and exergy losses occur in the brine re-injection unit. Ganjehsarabi et al. (2012) carried out the performance analysis of DORA-2 GPP which was performed by energy and exergy evaluations. The overall energetic ad exergetic efficiencies of the plant were found to be 10.7 % and 29.6 %, respectively. Dipippo (2004) used the Second Law of Thermodynamics as a comparison criteria of efficiency of different binary GPPs. Furthermore, Dipippo (2007) investigated ideal thermodynamic cycle which was appropriate for binary cycle GPPs. In this study, energy-based thermal efficiency was used as the measure of performance apart from the exergy-based utilization efficiency.

Thermodynamic analysis of binary cycle GPPs have been studied by many researchers. However, most of the authors considered that steam and NCGs content is zero through the cycle. The presented Thesis differs from the previous studies in that it considers NCGs effect and steam condensation through the cycle during mass and energy balances.

Electricity generation of a power plant is calculated by deterministic formulation. In literature, there are many studies on performance investigation of a GPP (Kanoglu and Bolatturk, 2008; Valdimarsson, 2003; Ganjehsarabi et al., 2012). However the data would be likelihood because inputs may be measured by uncalibrated devices or some parameters may be neglected during the calculation. Thus, the performance of power plant may be estimated by using regression analysis. An accurate estimate indicates whether the statuses of plant performance is over or lower than design conditions.

Regression analysis is used in a wide range of the scientific community such as in medicine, biology, econometric, engineering and social sciences (Ghani and Ahmad, 2010). If there is a relationship between two or more variables, which is not explained by any rule, this relation generally falls under the scope of statistics. One or more independent variables may affect a response variable in any case. Multiple linear regression analysis is a method of statistics in regression that is used to analyze the relationship between the single dependent variable with two or more independent variables.

In engineering, most of regression analysis studies related with energy are about prediction or understanding of energy consumption of buildings (Tso and Yau, 2007;

Kaza, 2010; Cho et al., 2004; Katipamula et al., 1994). Also, energy performance of buildings are evaluated and estimated with regression (Chung, 2012; Lee, 2010; Danov et al., 2012; Ghaiaus, 2006; Freire et al., 2008). In addition, cooling loads of air conditioning (HVAC) systems are modeled for buildings (Lam et al., 1997; Ben-Nakhi and Mahmoud, 2004; Lam et al., 2010). Besides these, regression analysis is often used to predict wind properties such as wind speed and direction (Salcedo-Sanz et al., 2011; Douak et al,. 2012; Utsunomiya et al., 1998). Several authors (Carta et al,. 2011; Amjady et al., 2011; Liu et al., 2013) studied estimation of power generation of a wind turbine.

Most studies in the related literature focus on regression analysis; none of them is associated with the estimation of electricity generation of a GPP. The estimation of instantaneous power generation in a GPP is very important to determine the performance status for plant operation. The present study, which is the first study to focus on the prediction of power generation of a GPP by regression, also utilizes multiple linear regression analysis of an existing binary GPP.

Air cooled binary cycle GPPs are generally the most appropriate selections for Turkey's geothermal resources because of water supply shortages. Therefore, thermodynamical and statistical performance models of an air cooled integrated two level binary cycle GPP is developed in the present study.

CHAPTER 4

SYSTEM

The DORA-1 GPP was in operation on May 2006 as the first binary power plant of Turkey. The plant type is the ITLU (integrated two level unit) air cooled binary cycle manufactured by Ormat. A general view of Dora-1 is shown in Figure 4.1.

Figure 4.1. General view of DORA-1 GPP

4.1. Balance of Plant (BOP)

The geothermal fluid is produced from AS-1 and ASR-2 productions wells, and reinjected to the AS-2 well. The enthalpies of the reservoir range between 660–680 kJ/kg with 1% NCG of the total flow. NCGs mainly consist of CO_2 and small amount of H_2S. The two-phase geothermal fluid is physically separated by the separators at each wellhead. After the separation, brine (geothermal fluid) firstly enters a tank and then is

pumped to the power plant by brine pumps. Separated steam and NCGs spontaneously go to the power plant by individual pipelines. A general view and flow diagram of wellhead equipment are provided in Figures 4.2 and 4.3, respectively.

Figure 4.2. Wellhead equipment of the ASR-2.

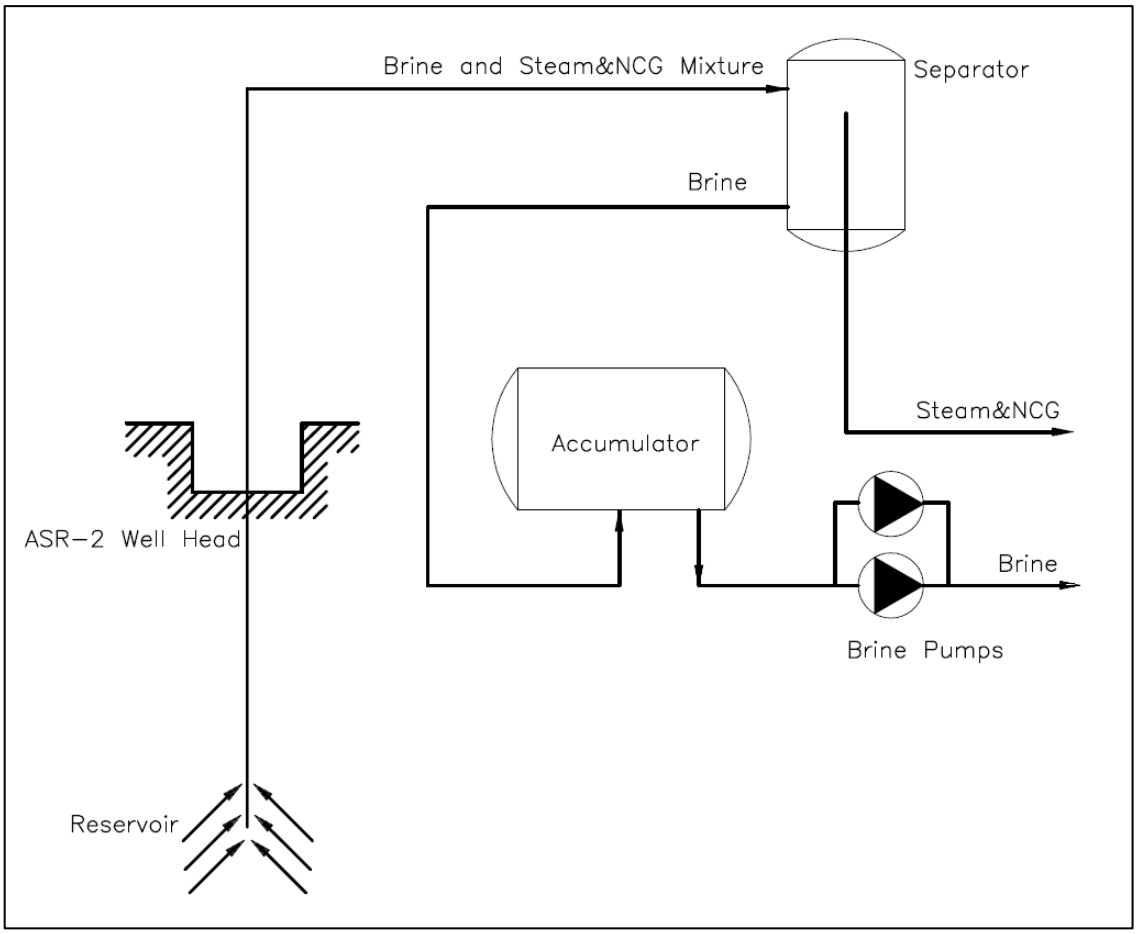

Figure 4.3. Flow diagram of the ASR-2.

4.2. Ormat Energy Converter (OEC)

The flow diagram of DORA-1 GPP is shown in Figure 4.4. The plant is divided into two Rankine cycle levels: Level 1 and Level 2. Although the working principles of these cycles are the same, their working pressures are different. N-pentane (C_5H_{12}) is the working fluid for both levels. The brine firstly enters the vaporizer of Level 1 where working fluid of Level 1 is heated. Then, it flows to the vaporizer of Level 2 to transfer its heat to the working fluid in this heat exchanger. Afterwards, the temperature of brine decreases and is divided equally into two for preheaters of level 1 and 2. In the preheaters, the brine temperature is further decreased and leaves the plant to be reinjected to AS-2 well. While the working fluid of Level 2 is vaporized by steam and NCGs, (through water vapor and NCGs tube section) which comes from the separator, the steam is condensed and pumped to the reinjection line by a condensate pump. NCGs

are vented from the vaporizer, sent to the liquid CO_2 plant, which is located next to the Plant.

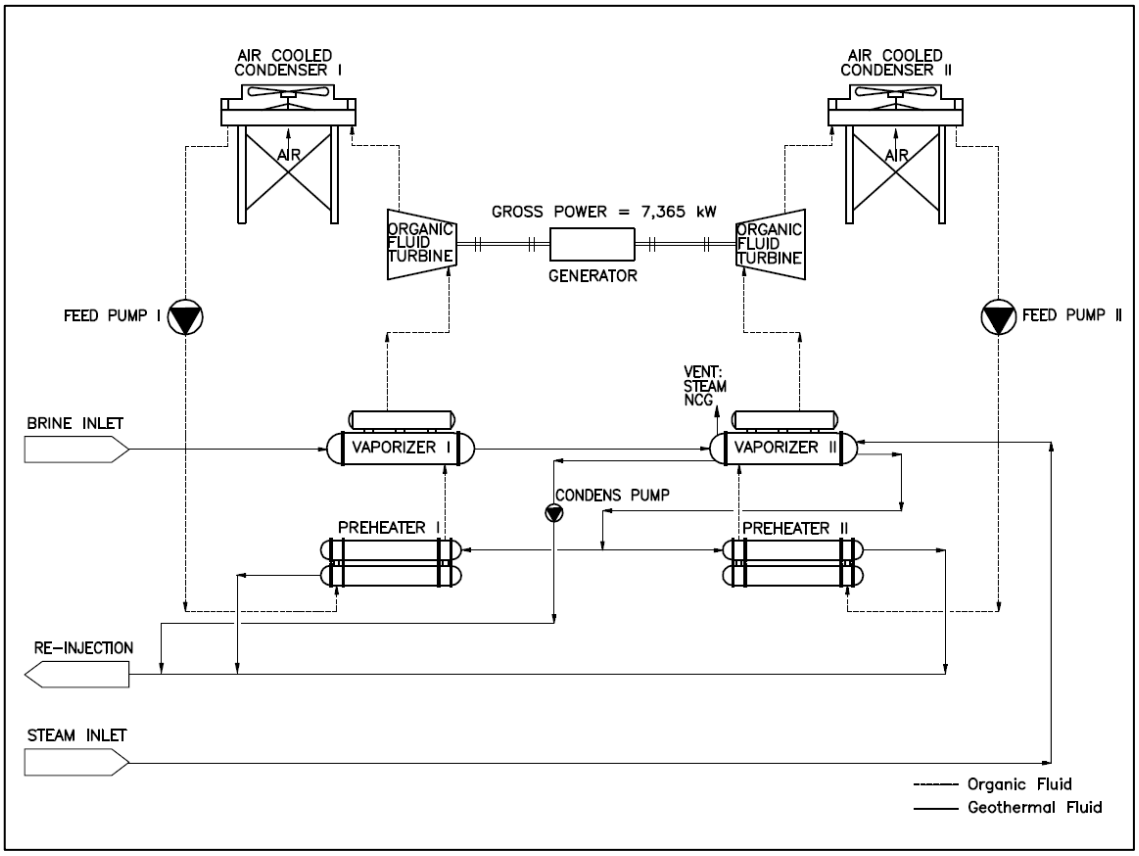

Figure 4.4. Flow diagram of DORA-1 GPP

In the vaporizers, the working fluid (n-pentane) is heated up to the boiling point. It evaporates, and then the superheated vapor enters the turbine, expands and its pressure decreases. The low-pressure vapor flows to an air-cooled condenser, where the vapor is condensed and then pumped back into the preheaters. Both levels have closed cycles and are independent from each other.

Design parameters of Dora-1 and their ranges are shown in Table 4.1.

Table 4.1. Design parameters of the Dora-1 plant
(source: Ormat, 2005; Toksoy et al., 2007).

Design parameters		Design ranges	
Ambient air temperature	17.1 °C	Amb. air temperature range	0–40°C
Brine flowrate	542.65 tons/hour	Brine flowrate range	80–110%
Vapor flowrate	22.45 tons/hour	Vapor flowrate range	80–110%
Brine temperature	157.9 °C	Brine Temperature range	150–166°C
Steam NCG content	33.6%	NCG content range	29–39%

The electricity is generated from the geothermal source at a temperature ranging from 157.9°C (plant inlet) to 78.9°C (reinjection). The total mass flowrate of the geothermal fluid, which comes from two production wells, is 565 tons/hour. The geothermal fluid has 22.45 tons/h steam which includes 33.6% NCG content. The Dora-1 GPP generates 7.35 MWe gross, 6.5 MWe net power at 17.1°C ambient air temperature and design conditions. After the electricity generation, NCGs are vented to produce liquid CO2 at another facility nearby the plant. In this facility, approximately 30,000 tons/year CO2 is liquefied and gained for beneficial uses (Linde Gas 2012, pers. commun.). The flowrate and temperature of the reinjection well is 557.55 tons/hour (brine+condensate) and 78.9°C, respectively.

CHAPTER 5

MODELING

The thermodynamic and regression models of a binary cycle geothermal power plant have been developed by using design parameters and data of DORA-1 GPP. Also, Ormat performance model is introduced in this chapter. Firstly, thermodynamic model of an air cooled binary cycle geothermal power plant is built by using five parameters: ambient air temperature, mass flow rate of brine, temperature of brine, mass flow rate of steam and steam NCGs content. After that, methodology of regression analysis is described and Ormat performance factors of DORA-1 GPP are briefly explained.

Method of calculation of thermodynamic model, regression analysis and Ormat performance model of DORA-1 GPP are given in this chapter.

5.1. Thermodynamic Model

5.1.1. Power Production Potential of a Geothermal Resource

Carnot cycle, which is also called ideal cycle, produces the highest thermal efficiency of any cycle operating between the geothermal reservoir temperature at T_H and low temperature source at T_L (DiPippo, 2007). A simple binary cycle geothermal power plant, which operates on the Carnot cycle, illustrated in Figure 5.1. Heat is transferred from the geothermal reservoir to the working fluid in the vaporizer and rejected from the working fluid to a sink (low-temperature source) (Sonntag et al, 2002).

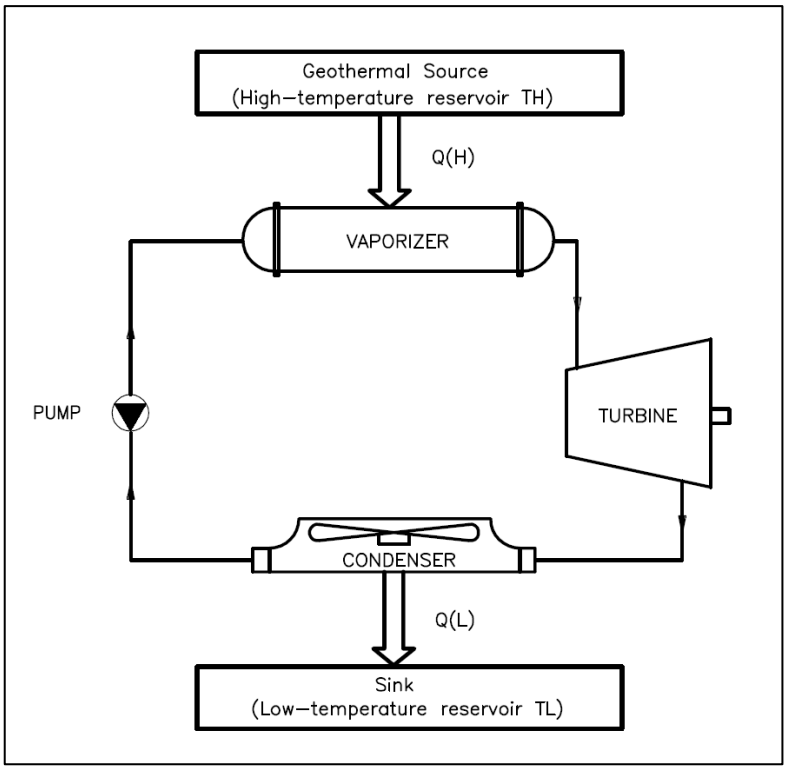

Figure 5.1. A simple Carnot cycle.

The maximum thermal efficiency of a thermal energy source that can be achieved is limited to the Carnot efficiency (Kanoglu, 2007). Carnot efficiency can be calculated as follows:

$$\eta_{carnot} = 1 - \frac{Q_L}{Q_H} = 1 - \frac{T_L}{T_H} \tag{5.1}$$

5.1.2. Mass and Energy Balance Equations

The first law of thermodynamics is related with conservation of energy. According to it, energy is a thermodynamic property (Çengel and Boles, 2005). The second law of thermodynamics is used to evaluate the performance of a plant by comparing the actual power output to the maximum theoretical power that could be produced from the given geothermal fluid. This involves determining the exergetic efficiency (Dipippo, 2005).

In this section, a theoretical air cooled binary cycle geothermal power plant is modeled by using design parameters of DORA-1 GPP according to the first law of thermodynamics.

Brine, steam and NCGs enter the heat exchangers for heating of working fluid. According to this process, temperature of this parameters decrease and most of steam condenses. Air is used for cooling of working fluid at the condenser. Main power consumption equipment is feed pumps, cooling fans and condensate pump which cause parasitic load. A block diagram for a mass and energy balance of an air cooled binary cycle GPP is illustrated in Figure 5.2.

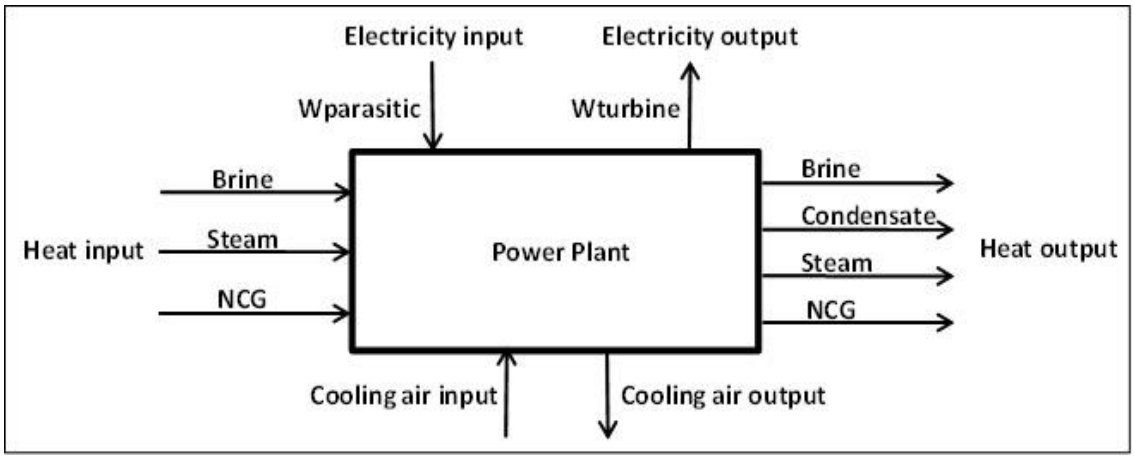

Figure 5.2. Block diagram of an air cooled binary cycle GPP.

Mass and energy balance equations for any control volume at steady-state, steady-flow process can be expressed in Table 5.1.

Table 5.1. Mass and energy balance equations of the model.

	Equations	Equation Number
Mass	$\dot{m}_{in} = \dot{m}_{brine} + \dot{m}_{steam} + \dot{m}_{NCG}$	(5.2)
	$\dot{m}_{out} = \dot{m}_{brine} + \dot{m}_{condensate} + \dot{m}_{unusedsteam} + \dot{m}_{NCG}$	(5.3)
	$\sum \dot{m}_{in} = \sum \dot{m}_{out}$	(5.4)
Energy	$\dot{Q}_{net,in} - \dot{W}_{net} = \sum \dot{m}_{out} h_{out} - \sum \dot{m}_{in} h_{in}$	(5.5)
	$\dot{Q}_{net,in} = \dot{Q}_{in} - \dot{Q}_{out}$	(5.6)
	$\dot{W}_{parasitic} = \dot{W}_{pump} + \dot{W}_{condens\,pump} + \dot{W}_{condenser\,fans}$	(5.7)
	$\dot{W}_{net} = \dot{W}_{gen} - \dot{W}_{parasitic}$	(5.8)

Energy or thermal efficiency of power plants which are converted of thermal energy to electricity is defined as the ratio of provided thermal energy by generated electricity (Kanoglu, 2007). The thermal efficiency of the plant can be expressed as:

$$\eta_{plant} = \frac{\dot{W}_{net}}{\dot{Q}_{ph1} + \dot{Q}_{ph2} + \dot{Q}_{vap1} + \dot{Q}_{vap2}} \tag{5.9}$$

ε-NTU method is utilized to carry out of the heating and cooling process calculations of the heat exchangers (Kakac and Liu, 1998):

$$\mathrm{C_h} = \dot{\mathrm{m}}_\mathrm{h} \mathrm{c_{p,h}} \tag{5.10}$$

$$\mathrm{C_c} = \dot{\mathrm{m}}_\mathrm{c} \mathrm{c_{p,c}} \tag{5.11}$$

$$\mathrm{C_{min}} = \min(\mathrm{C_h}, \mathrm{C_c}) \tag{5.12}$$

$$\dot{\mathrm{Q}} = \varepsilon\, \mathrm{C_{min}} \left(\mathrm{T_{h,in}} - \mathrm{T_{c,in}}\right) \tag{5.13}$$

$$\mathrm{T_{h,out}} = \mathrm{T_{h,in}} - \dot{\mathrm{Q}}/\mathrm{C_h} \tag{5.14}$$

$$\mathrm{T_{c,out}} = \mathrm{T_{c,in}} + \dot{\mathrm{Q}}/\mathrm{C_c} \tag{5.15}$$

where subscriptions h and c represent the hot and cold fluids. C_h, $\dot{m}_h$, $c_{p,h}$ and C_c, $\dot{m}_c$, $c_{p,c}$ are the heat capacities, mass flow rates and specific heat capacities of hot and cold fluids, respectively. T is the temperature and ε, which is calculated by using real data of DORA-1 GPP, is the effectiveness of heat exchangers.

In the following part, mass and energy balance equations of all plant components, which are preheaters, vaporizers, turbines, condensers and feed pumps, are introduced.

5.1.2.1. Vaporizers

The vaporizers of DORA-1 GPP are designed as horizontal shell and tube heat exchangers. Brine flows through the tube section of the vaporizers with four passes at level I and level II. Steam and NCGs only flow through the bottom tube section of level II with single pass. Steam condenses in the vaporizer of level II and is pumped to reinjection pipe line by a condensate pump. NCG are released from end of the vaporizer with unused steam. They are sent to another company to produce CO_2. N-pentane flows through the shell section of vaporizers with two passes for level I and a single pass for level II (Ormat, 2004).

Simple schematic and flow diagram of level I vaporizer is illustrated in Figure 5.3.

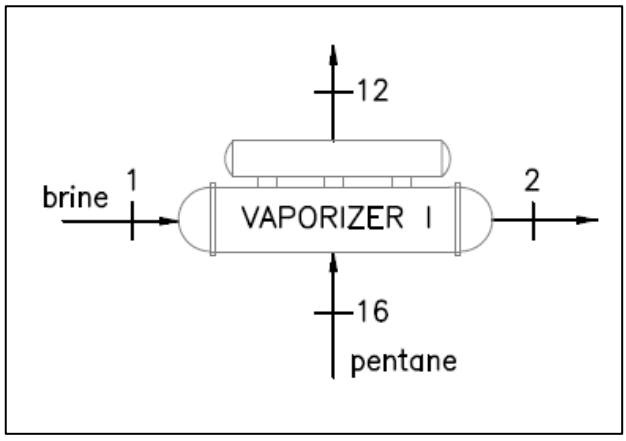

Figure 5.3. Flow diagram of Level I vaporizer.

Figure 5.4 is the diagram showing the heat exchange process between the brine and the working fluid n-pentane in Level I vaporizer. The states refer to Figure 5.3. The x-axis represents the path of the fluid flow in the heat exchanger.

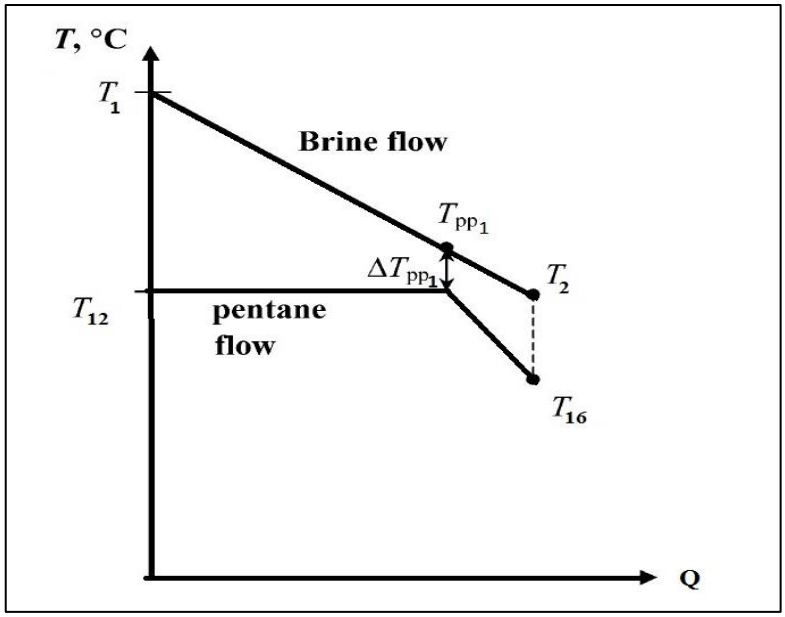

Figure 5.4. Temperature and heat transfer diagram between the brine and the n-pentane in Level I vaporizer.

According to $\varepsilon - NTU$ method, heat transfer of level I vaporizer can be calculated for heating by equations:

$$C_1 = \dot{m}_1 * c_{p,1} \tag{5.16}$$

$$C_{16} = \dot{m}_{pentane,1} * c_{p,16} \tag{5.17}$$

$$\mathrm{C_{min,vap1}} = \min(\mathrm{C_1}, \mathrm{C_{16}}) \tag{5.18}$$

$$\dot{Q}_{vap1,heating} = \varepsilon_{vap1} C_{min,vap1}\left(T_{pp1} - T_{16}\right) \tag{5.19}$$

$$\mathrm{T_2} = \mathrm{T_{pp1}} - \dot{Q}_{vap1,heating}/\mathrm{C_1} \tag{5.20}$$

$$\mathrm{T_{12}} = \mathrm{T_{16}} + \dot{Q}_{vap1,heating}/\mathrm{C_{16}} \tag{5.21}$$

Heat transfer during boiling is calculated as:

$$\dot{Q}_{vap1,boiling} = \dot{m}_{pentane,1}\left(h_{12g} - h_{12f}\right) = C_1\left(T_1 - T_{pp1}\right) \tag{5.22}$$

Total heat transfer of level I vaporizer is:

$$\dot{Q}_{vap1} = \dot{Q}_{vap1,heating} + \dot{Q}_{vap1,boiling} \tag{5.23}$$

Design of level II vaporizer is quite different from level I vaporizer because steam and NCGs flows through the tube section of vaporizer as well as brine. Simple schematic and flow diagram of level II vaporizer is shown in Figure 5.5.

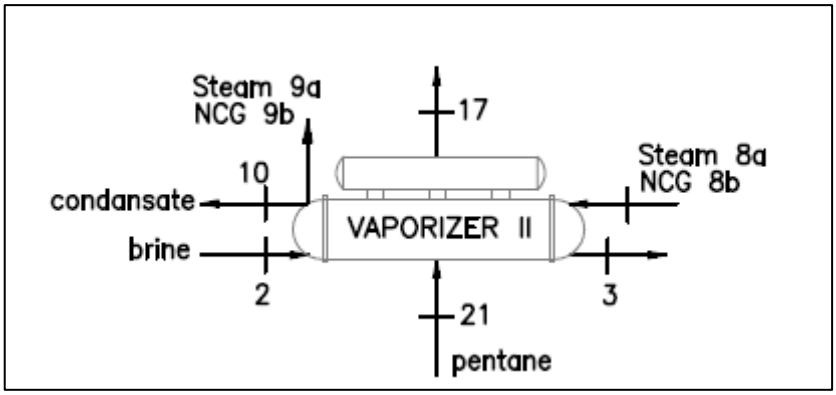

Figure 5.5. Flow diagram of Level II vaporizer.

Heat exchanging process in Level II vaporizer, which heat transferred from the brine, steam and NCGs to n-pentane, is shown in Figure 5.6.

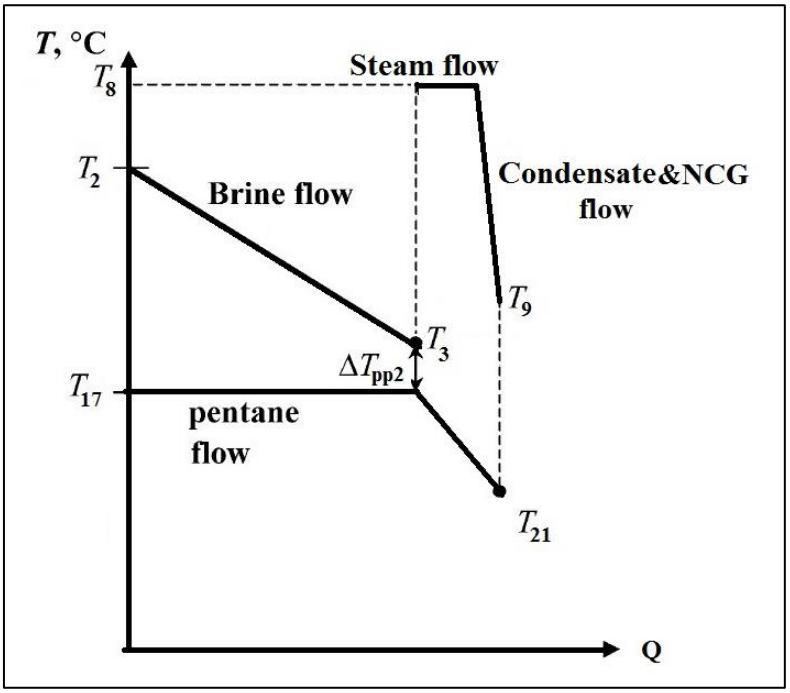

Figure 5.6. Temperature and heat transfer diagram between the brine+steam+NCG and the n-pentane in Level II vaporizer.

According to $\varepsilon - NTU$ method, heat transfer of level II vaporizer can be calculated for heating by equations:

$$C_8 = \dot{m}_8 * c_{p,8} \tag{5.24}$$

$$C_{21} = \dot{m}_{pentane2} * c_{p,21} \tag{5.25}$$

$$\mathrm{C_{min,vap2}} = \min(\mathrm{C_8}, \mathrm{C_{21}}) \tag{5.26}$$

$$\dot{Q}_{vap2,heating} = \varepsilon_{vap2} C_{min,vap2} (T_8 - T_{21}) \tag{5.27}$$

$$\mathrm{T_9} = \mathrm{T_8} - \dot{Q}_{vap2,heating}/\mathrm{C_8} \tag{5.28}$$

$$\mathrm{T_{17}} = \mathrm{T_{21}} + \dot{Q}_{vap2,heating}/\mathrm{C_{21}} \tag{5.29}$$

Heat transfer during boiling is calculated as:

$$\dot{Q}_{vap2,boiling} = \dot{m}_{pentane2}\left(h_{17g} - h_{17f}\right) = C_2(T_2 - T_3) \tag{5.30}$$

$$T_{pp2} = T_3 - T_{17} \tag{5.31}$$

Total heat transfer of level II vaporizer is:

$$\dot{Q}_{vap2} = \dot{Q}_{vap2,heating} + \dot{Q}_{vap2,boiling} \tag{5.32}$$

5.1.2.2. Preheaters

The preheaters are also designed as horizontal shell and tube heat exchangers. The tube section has two-pass construction, through which brine flows. N-pentane flows through the shell section with two passes (Ormat, 2004).

The flow diagram of level I preheater is shown in Figure 5.7.

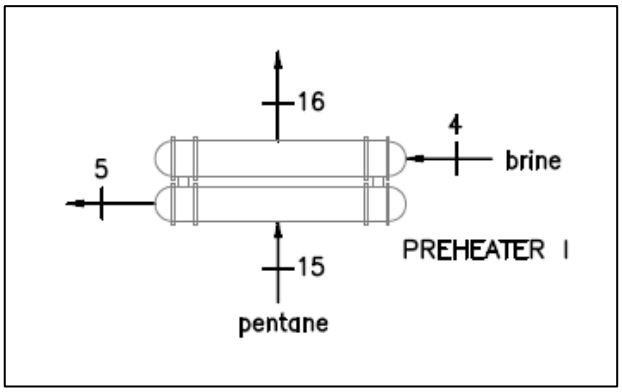

Figure 5.7. Flow diagram of Level-I preheater.

In preheaters, the brine only heats and is increase of temperature of working fluid. There is no boiling in the preheaters. Temperature and heat diagram of level I preheater is shown in Figure 5.8.

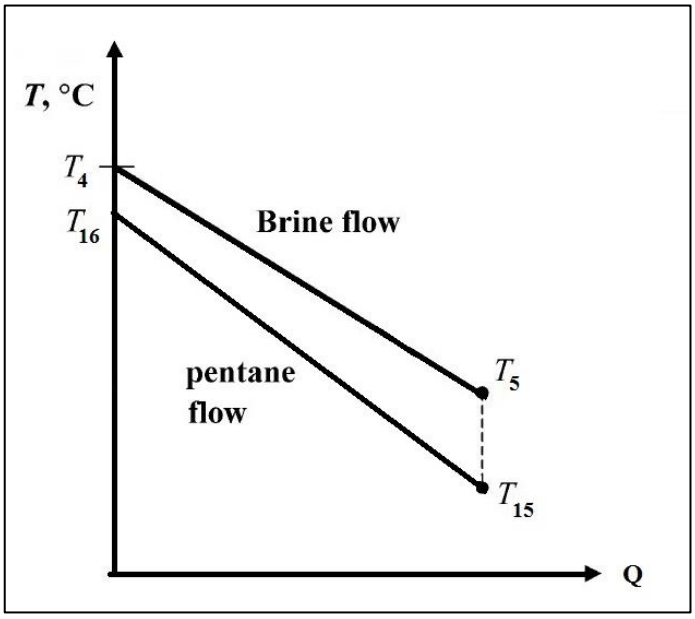

Figure 5.8. Temperature and heat transfer diagram between the brine and the n-pentane in Level I preheater.

According to ε-NTU method, heat transfer is calculated as:

$$C_4 = \dot{m}_4 * c_{p,4} \tag{5.33}$$

$$C_{15} = \dot{m}_{pentane1} * c_{p,15} \tag{5.34}$$

$$\mathrm{C_{min,ph1}} = \min(\mathrm{C_4}, \mathrm{C_{15}}) \tag{5.35}$$

$$\dot{\mathrm{Q}}_{\mathrm{ph1}} = \varepsilon_{\mathrm{ph1}} \mathrm{C_{min,ph1}} (\mathrm{T_4} - \mathrm{T_{15}}) \tag{5.36}$$

$$T_5 = T_4 - \dot{Q}_{ph1}/C_4 \quad (5.37)$$

$$T_{16} = T_{15} + \dot{Q}_{ph1}/C_{15} \quad (5.38)$$

The flow diagram of level II preheater is shown in Figure 5.9.

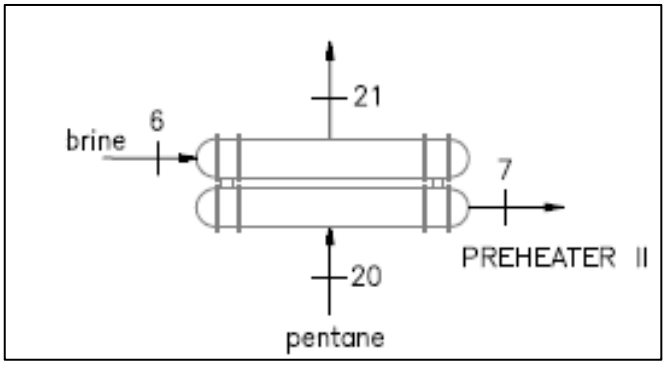

Figure 5.9. Flow diagram of Level II preheater.

Temperature and heat diagram of level II preheater is shown in Figure 5.10.

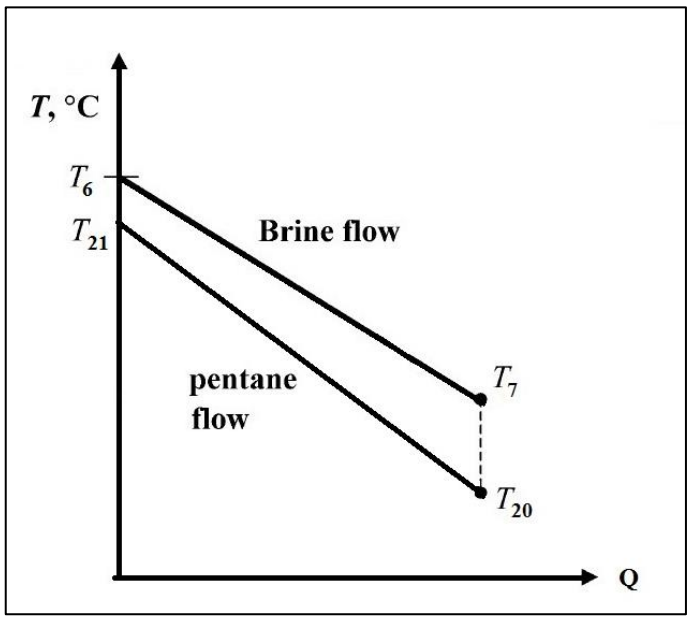

Figure 5.10. Temperature and heat transfer diagram between the brine and the n-pentane in Level II preheater.

Heat transfer between the brine and n-pentane in level II preheater is calculated as:

$$C_6 = \dot{m}_6 * c_{p,6} \tag{5.39}$$

$$C_{20} = \dot{m}_{pentane2} * c_{p,20} \tag{5.40}$$

$$\mathrm{C_{min,ph2}} = \min(\mathrm{C_6}, \mathrm{C_{20}}) \tag{5.41}$$

$$\dot{\mathrm{Q}}_{\mathrm{ph2}} = \varepsilon_{\mathrm{ph2}} \mathrm{C_{min,ph2}} (\mathrm{T_6} - \mathrm{T_{20}}) \tag{5.42}$$

$$\mathrm{T_7} = \mathrm{T_6} - \dot{\mathrm{Q}}_{\mathrm{ph2}} / \mathrm{C_6} \tag{5.43}$$

$$\mathrm{T_{21}} = \mathrm{T_{20}} + \dot{Q}_{ph2} / \mathrm{C_{20}} \tag{5.44}$$

5.1.2.3. Turbines and Generator

In the vaporizers, the working fluid is heated up to boiling point and evaporates. Then superheated vapor enters the organic turbine, drives a set of blades to rotate a shaft and expands. Thus, this process results on decrease in pressure and temperature as well as the production of rotational shaft power by transforming kinetic energy gained by expansion of vapor process. Simple schematic of turbines and synchronous generator is illustrated in Figure 5.11.

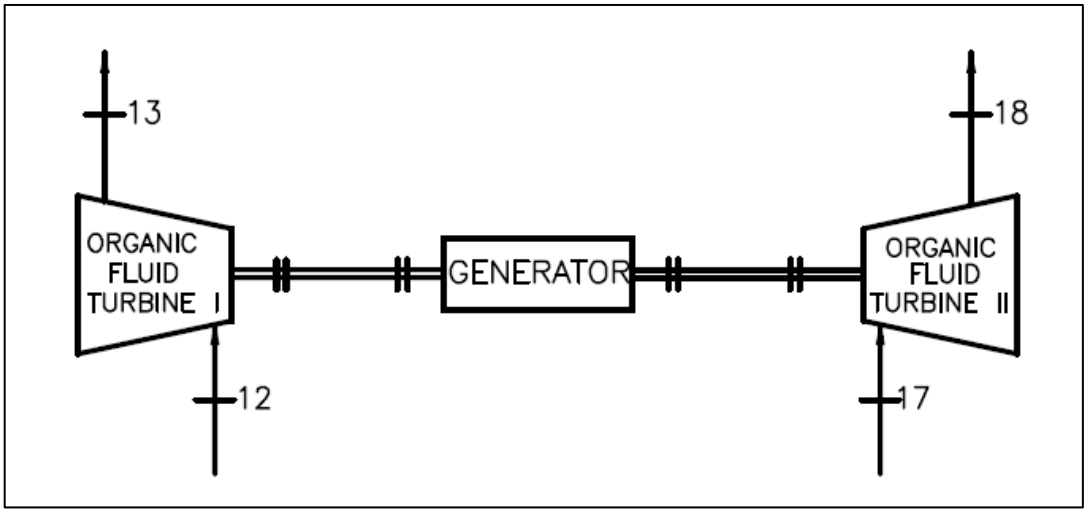

Figure 5.11. Simple schematic of turbines and generator.

Turbine power is calculated with assuming negligible potential and kinetic energy at steady-state, steady flow, in adiabatic operation (Dipippo, 2004).

For Level 1:

$$\dot{W}_{turb1} = \dot{m}_{pentane1}(h_{12} - h_{13}) = \dot{m}_{pentane1}\,\eta_{turb,s1}(h_{12} - h_{13s}) \tag{5.45}$$

where $\eta_{turb,s}$ is the isentropic turbine efficiency.

$$n_{turb,s1} = \frac{h_{12} - h_{13}}{h_{12} - h_{13s}} \tag{5.46}$$

For Level 2:

$$\dot{W}_{turb2} = \dot{m}_{pentane2}(h_{17} - h_{18}) = \dot{m}_{pentane2}\,\eta_{turb,s2}(h_{17} - h_{18s}) \tag{5.47}$$

$$n_{turb,s2} = \frac{h_{17} - h_{18}}{h_{17} - h_{18s}} \tag{5.48}$$

Generator power is calculated as:

$$\dot{W}_{gen} = \left(\dot{W}_{turb1} + \dot{W}_{turb2}\right).\eta_{gen} \tag{5.49}$$

where η_{gen} is the generator efficiency during transmission of the rotational shaft power.

5.1.2.4. Air Cooled Condensers

The condensers are horizontal air cooled heat exchangers that contains thirty fans on the tube bundles. Fans, is transferred air from under of tube bundles to atmosphere, are driven by electric motors (Ormat, 2004).

After the turbine, low pressure vapor flows to the air cooled condenser and it is cooled and condensed. Flow diagram of the air cooled condensers is shown Figure 5.12.

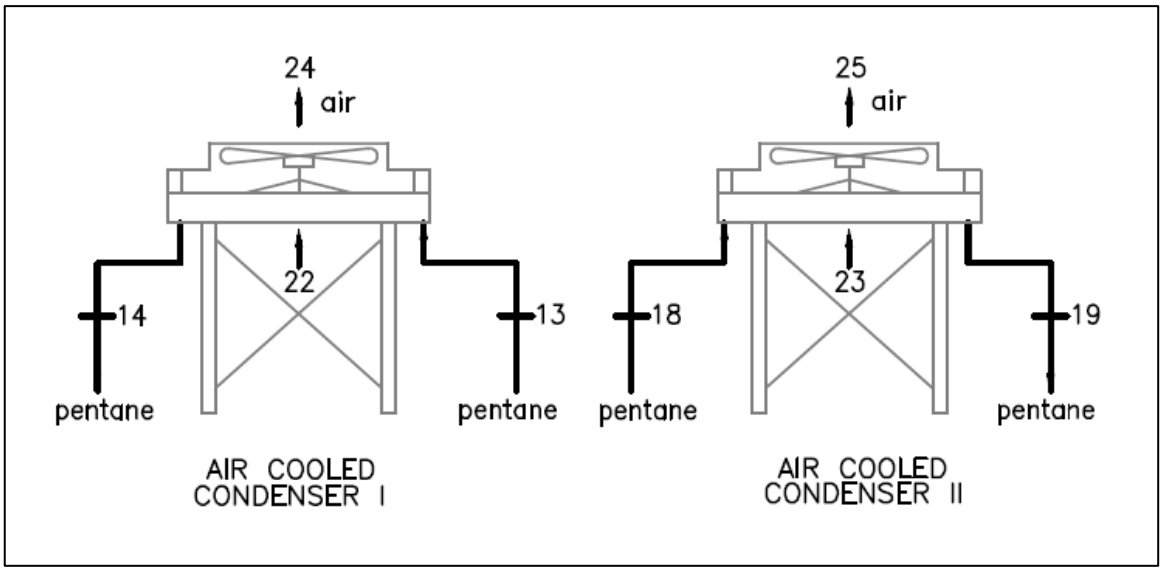

Figure 5.12. Flow diagram of condensers.

Each level uses 15 fans with three rows for cooling and condensing. Top view of the condenser is illustrated in Figure 5.13.

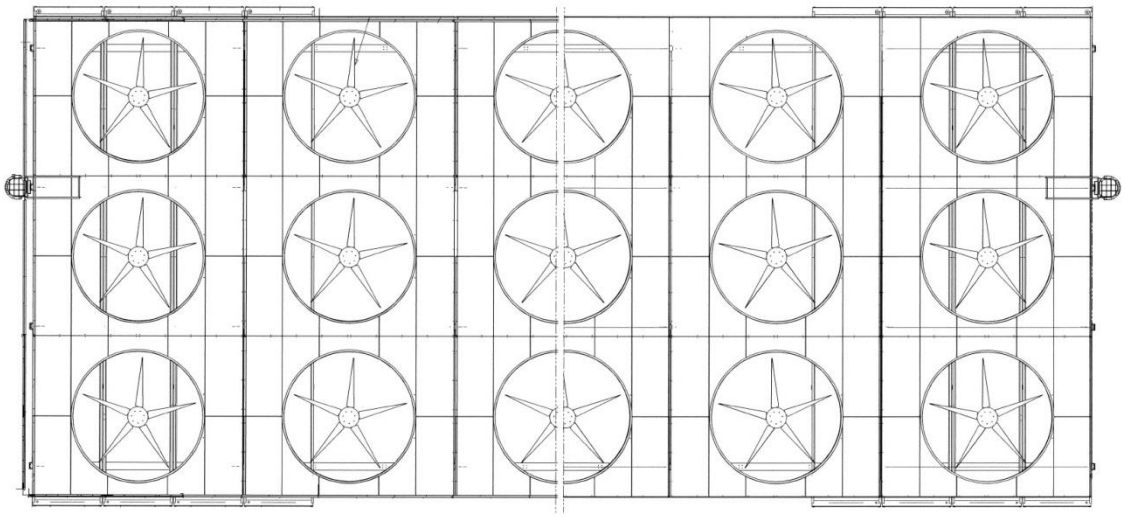

Figure 5.13. Top view of condenser for each level.

The pentane temperature is assumed as cools down while passing through the first five fans. Other fans are used for condensing.

Heat transfer between the air and n-pentane at condensers is calculated as:

For Level 1:

$$C_{22} = \dot{m}_{22} * 5 * c_{p,22} \quad (5.50)$$

$$C_{13} = \dot{m}_{pentane,1} * c_{p,13} \quad (5.51)$$

$$\mathrm{C_{min,cond1}} = \min(\mathrm{C_{22}}, \mathrm{C_{13}}) \quad (5.52)$$

$$\dot{Q}_{cond1,cooling} = \varepsilon_{cond1} C_{min,cond1} (T_{13} - T_{22}) \quad (5.53)$$

$$\mathrm{T_{14}} = \mathrm{T_{13}} - \dot{Q}_{cond1,cooling}/\mathrm{C_{13}} \quad (5.54)$$

$$\mathrm{T_{24}} = \mathrm{T_{22}} + \dot{Q}_{cond1,cooling}/\mathrm{C_{22}} \quad (5.55)$$

Heat transfer during condensing is calculated as:

$$\dot{Q}_{cond1,condensing} = \dot{m}_{pentane,1}(h_{14g} - h_{14f}) = \dot{m}_{22}.10.c_{22.}(T_{24,2} - T_{22}) \quad (5.56)$$

Total heat transfer of level I condenser is:

$$\dot{Q}_{cond1} = \dot{Q}_{cond1,cooling} + \dot{Q}_{cond1,condensing} \quad (5.57)$$

For Level 2:

$$C_{23} = \dot{m}_{23} * 5 * c_{p,23} \quad (5.58)$$

$$C_{18} = \dot{m}_{pentane,2} * c_{p,18} \quad (5.59)$$

$$\mathrm{C_{min,cond2}} = \min(\mathrm{C_{23}}, \mathrm{C_{18}}) \quad (5.60)$$

$$\dot{Q}_{cond2,cooling} = \varepsilon_{cond2} C_{min,cond2} (T_{18} - T_{23}) \quad (5.61)$$

$$\mathrm{T_{19}} = \mathrm{T_{18}} - \dot{Q}_{cond2,cooling}/\mathrm{C_{18}} \quad (5.62)$$

$$\mathrm{T_{25}} = \mathrm{T_{23}} + \dot{Q}_{cond2,cooling}/\mathrm{C_{23}} \quad (5.63)$$

Heat transfer during condensing is calculated as:

$$\dot{Q}_{cond2,condensing} = \dot{m}_{pentane,2}(h_{19g} - h_{19f}) = \dot{m}_{23}.10.c_{23.}(T_{25,2} - T_{23}) \quad (5.64)$$

Total heat transfer of level II condenser is:

$$\dot{Q}_{cond2} = \dot{Q}_{cond2,cooling} + \dot{Q}_{cond2,condensing} \qquad (5.65)$$

5.1.2.5. Feed Pumps

Two multistage centrifugal feed pumps are used to transfer of n-pentane from condensers to the preheater. Flow diagram of feed pumps is illustrated in Figure 5.14.

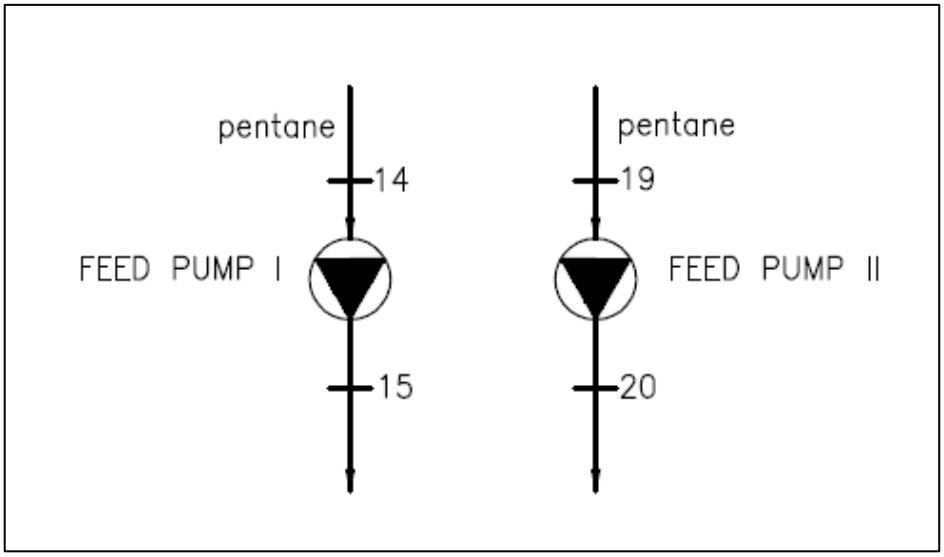

Figure 5.14. Flow diagram of feed pumps.

Energy consumptions of the feed pumps are calculated with assuming negligible potential and kinetic energy at steady-state, steady flow, in adiabatic operation (Dipippo, 2004):

For Level 1:

$$\dot{W}_{pump1} = \dot{m}_{pentane1}(h_{15} - h_{14}) = \dot{m}_{pentane1}\,\eta_{pump,s1}(h_{15s} - h_{14}) \qquad (5.66)$$

where $n_{pump,s}$, is the isentropic pump efficiency.

$$n_{pump,s1} = \frac{h_{15s} - h_{14}}{h_{15} - h_{14}} \qquad (5.67)$$

For Level 2:

$$\dot{W}_{pump2} = \dot{m}_{pentane2}(h_{20} - h_{19}) = \dot{m}_{pentane2}\,\eta_{pump,s2}(h_{20s} - h_{19}) \qquad (5.68)$$

$$n_{pump,s2} = \frac{h_{20s} - h_{19}}{h_{20} - h_{19}} \qquad (5.69)$$

Total feed pump work can be calculated as:

$$\dot{W}_{pump} = \dot{W}_{pump1} + \dot{W}_{pump2} \qquad (5.70)$$

5.2. Regression Model

The performance of a power plant could be estimated by using regression analysis. An accurate estimate indicates whether the status of plant performance is higher or lower than design conditions.

Power generation from a geothermal resource is limited between thermo physical properties of high temperature heat resource (geothermal reservoir) and low temperature heat source (air). Temperature, pressure, mass flow rate of geothermal fluid and its contents (vapor and Non-condensable gases) and temperature of air directly affect the performance of plant.

This chapter investigates methodology of multiple linear regression analysis for data of DORA-1 GPP.

5.2.2. Theoretical Considerations

The dependent variable is the net power production of the plant while the ambient air temperature, the brine mass flow rate and the brine inlet temperature are the independent variables. Multiple linear regression model of the net power production can be written as follows (Celik, 2011; Drapper and Smith, 1998):

$$\begin{bmatrix} Y_1 \\ Y_2 \\ \vdots \\ \vdots \\ Y_N \end{bmatrix} = \begin{bmatrix} 1 & X_{12} & X_{13} & \dots & \dots & X_{1N} \\ 1 & X_{22} & X_{23} & \dots & \dots & X_{2N} \\ \vdots & \vdots & \vdots & \dots & \dots & \vdots \\ \vdots & \vdots & \vdots & \dots & \dots & \vdots \\ 1 & X_{N2} & X_{N3} & \dots & \dots & X_{NK} \end{bmatrix} \times \begin{bmatrix} \beta_1 \\ \beta_2 \\ \vdots \\ \vdots \\ \beta_N \end{bmatrix} + \begin{bmatrix} \varepsilon_1 \\ \varepsilon_2 \\ \vdots \\ \vdots \\ \varepsilon_N \end{bmatrix} \quad (5.71)$$

$$Y_i = \beta_0 + \beta_1 X_1 + \beta_2 X_2 + \cdots + \beta_N X_N + \varepsilon_i \quad (5.72)$$

In this model, Y is dependent variable, X's are independent variables, β_0 regression constant, $\beta_1, \beta_2, \ldots, \beta_N$ are partial regression coefficients and ε_i is error term. Generally, least squares method is used to estimate β's in the regression analysis. β coefficients and error term (ε), which are difficult and changeable for each prediction of Y, are easily evaluated by this method. Therefore instead of real β coefficient, the least square estimators of β's, which are b's, are calculated. An error function is presented by the following equation.

$$\varepsilon = Y - X\beta \quad (5.73)$$

To get the square of a matrix, it is multiplied by the transpose of itself, the error sum of squares can be calculated in equation 5.74.

$$S_\beta = \varepsilon\, \varepsilon' = (Y - X\beta)(Y - X\beta)' \quad (5.74)$$

$$S_\beta = Y'Y - 2\beta'X'Y + \beta'X'X\beta \quad (5.75)$$

When the derivation of error sum of squares taken according to β is taken, the least square estimators of β's (b's) are calculated by equation 5.76.

$$b = (X'X)^{-1}X'Y \quad (5.76)$$

$$Y_i = b_0 + b_1 X_1 + b_2 X_2 + \cdots + b_N X_N + \varepsilon_i \quad (5.77)$$

5.2.3. Assumptions of the Classical Linear Regression Model

While building a forecasting model in multiple linear regression analysis, the basic assumptions of classical linear regression should be checked. There are generally six assumptions regarding the multiple linear regression analysis: normality, zero mean and normal distribution of errors, linearity, homoscedasticity, no-multicollinearity and no-autocorrelation (Celik, 2011; Gujarati, 2003; Drapper and Smith, 1998).

The first assumption is related to normality. This means that each of the independent variables should have a normal distribution. Normality of independent variables can be checked by Kurtosis and Skewness distributions. The results of distributions should be between -1.0 and +1.0. If the distribution of the variable is not normal, transformation of the independent variable may be necessary (Ghani and Ahmad, 2010).

The second assumption is that errors has zero mean and normally distributed (Figure 5.15).

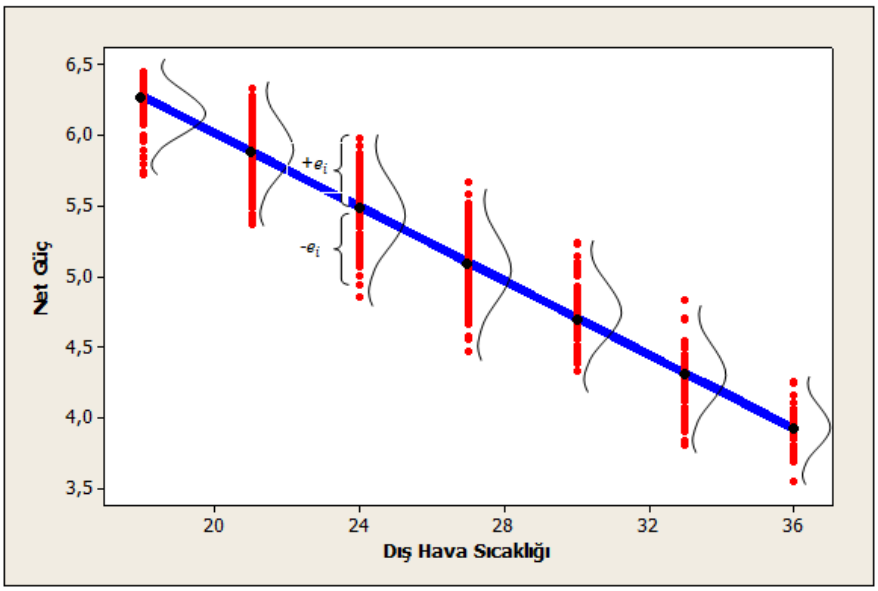

Figure 5.15. The variance of each normal distribution is assume to be the same variance.

The third assumption “linearity”, focuses on linear relationship between the dependent and the independent variables. Hypothesis tests should be applied to learn whether there exist a linear relationship between these variables. The coefficient of the controlled variables is checked by a test statistic and insignificant variables should be

removed from the model. After that, F-test is applied to decide that the model is useful or not.

The structure of hypothesis testing for models can be built to control F-testing as follows:

$H_0: b_1 = b_2 = b_3 = b_4 = 0$

$H_A: b_i \neq 0$ (at least one)

According to the null hypothesis, none of the independent variables is significantly related to the dependent variable. But an alternative hypothesis is that at least one of the independent variable is significantly related to the dependent variable at the α = 0.05 level of significance.

The fourth assumption is that all data should be free from heteroscedasticity. If each of the errors has same (constant) variance, regression is in homoscedasticity. In this assumption, residual analysis needs to be investigated (Eq: 5.78-5.80).

$$\mathrm{Var}(\varepsilon_i) = \sigma^2 \tag{5.78}$$

$$\mathrm{Cov}(\varepsilon_i, \varepsilon_j) = 0 \tag{5.79}$$

$$\begin{bmatrix} \mathrm{Var}(\varepsilon_1) & \mathrm{Cov}(\varepsilon_1, \varepsilon_2) & \dots & \mathrm{Cov}(\varepsilon_1, \varepsilon_4) \\ \mathrm{Cov}(\varepsilon_2, \varepsilon_1) & \mathrm{Var}(\varepsilon_2) & \dots & \mathrm{Cov}(\varepsilon_2, \varepsilon_4) \\ \vdots & \vdots & \ddots & \vdots \\ \mathrm{Cov}(\varepsilon_n, \varepsilon_1) & \mathrm{Cov}(\varepsilon_n, \varepsilon_2) & \mathrm{Cov}(\varepsilon_n, \varepsilon_3) & \mathrm{Var}(\varepsilon_n) \end{bmatrix} = \begin{bmatrix} \sigma^2 & 0 & \dots & 0 \\ 0 & \sigma^2 & \dots & 0 \\ \vdots & \vdots & \ddots & \vdots \\ 0 & 0 & \dots & \sigma^2 \end{bmatrix} \tag{5.80}$$

Forecasting model can be checked whether there is heteroscedasticity between residuals and the response variable or the controlled variables by Breusch-Pagan and Koenker methods (Breusch and Pagan, 1979; WWW_spsstools, 2012). Generally, heteroscedasticity test is not necessary for time series data.

The fifth assumption that should be checked in research is multicollinearity. Multicollinearity occurs when there is high degree of correlation among the controlled variables. Variance Inflation Factor (VIF) is used for measuring the degree of multicollinearity of the independent variable with the other independent variables in a regression model (Eq. 5.81) (O'Brien, 2007).

$$\mathrm{VIF}(b_i) = \frac{1}{1 - {R_i}^2} \tag{5.81}$$

When the value of VIF is less than 5, it is obvious that multicollinearity is not serious. If VIF is more than 5, then multicollinearity is substantial. It will be more serious whenever the value of VIF is more than 10.

Finally, Durbin–Watson statistic (d) should be used to check autocorrelation (Eq. 5.82). Durbin-Watson is a test statistic which is used to detect the presence of autocorrelation among the errors from a regression analysis (Drapper and Smith, 1998).

$$d = \sum_{u=2}^{N} (\varepsilon_u - \varepsilon_{u-1})^2 \Big/ \sum_{u=1}^{N} {\varepsilon_u}^2 \tag{5.82}$$

The value of d always lies between 0 and 4. When d = 2, it indicates no autocorrelation. If the Durbin–Watson statistic is substantially less than 2, there is evidence a positive serial correlation. If d > 2, successive error terms are much different in value to one another, so it is negatively correlated. If there is an autocorrelation in the model, the model can be eliminated by Orcutt-Cochran Method and Prais-Winsten Procedure (Prais and Winsten, 1954; Cochrane and Orcutt, 1949)

5.3. Ormat Performance Model

Ormat is the manufacturer of DORA-1 GPP. Performance factors of the plant and its calculation procedures were given by Ormat (Ormat, 2005). These factors and procedures are explained in this part.

5.3.1. Performance Correction Factors

Performance correction factors, which are given by DORA-1's manufacturer Ormat, are used to determine plant performance and whether the design values. Each of the correction factors are computerized as a polynomial function by Ormat. Correction factor functions of DORA-1 GPP are shown in Table 5.2.

Table 5.2. Correction factor functions of the DORA-1 GPP.

Description	Factor	Function	Equation Number
Ambient air temperature correction factor	F_1	$a + bT_{air} + cT_{air}^2 + dT_{air}^3$	(5.83)
Steam flow rate correction factor	F_2	$a + b.SF + c.SF^2$	(5.84)
Steam NCGs content correction factor	F_3	$a + bNCG + cNCG^2$	(5.85)
Brine flow rate correction factor	F_4	$a + bBF + cBF^2 + dBF^3$	(5.86)
Brine inlet temperature correction factor	F_5	$a + bT_{brine} + cT_{brine}^2 + dT_{brine}^3$	(5.87)

The coefficients of the performance correction factors are shown in Table 5.3.

Table 5.3. Correction factor coefficients.

Performance Correction Factors	Coefficients			
	a	b	c	d
$F_1(0 < T_{air} < 17.1)$	1,199496898	-0,00165519	-0,00091925	0,000019520313
$F_1(17.1 < T_{air} < 40)$	1,266370843	-0,00818416	-0,00052288	5,29433E-06
F_2	0,712045851	0,455304413	-0,16735026	0
F_3	0,918027028	0,737766183	-1,46896962	0
F_4	1,379782213	-3,59934501	5,495023224	-2,275460428
F_5	-29,073832	0,465757096	-0,00237107	3,97446E-06

CHAPTER 6

RESULTS AND DISCUSSION

6.1. Thermodynamic Model

6.1.1. Assumptions and constants

Before modeling of a power plant, some assumptions should be made in advance. These assumptions are:

- The system of the geothermal plant is considered for any control volume at steady state with negligible kinetic and potential energy changes.
- Air, which is accepted as ideal gas, is in homogeneous distribution in the air cooled condenser.
- The properties of geothermal fluid are taken as water.
- The turbines and pumps have isentropic efficiencies.

Also, some values in the Table 6.1 are assumed as constant to evaluate thermodynamic calculation due to modeling of the power plant. These constants, which are real data of DORA-1 GPP, are calculated from a real binary power plant.

Table 6.1. Some constants for model.

Parameter	**Value**	**Unit**
Reservoir temperature	157.9	°C
Mass flow rate of brine	542.65	ton/hr
Well head pressure	7	bar
Brine pump pressure	8	bar
Mass flow rate of steam	22.45	ton/hr
NCG content in the steam	33.6	%
Turbine isentropic efficiency	80	%
Feed pump isentropic efficiency	80	%
Effectiveness of air cooled condenser*	70	%
Effectiveness of vaporizer 1*	90	%
Effectiveness of vaporizer 2*	90	%

Table 6.1. Some constants for model (cont.)

Effectiveness of preheaters*	90	%
Ambient air temperature	17.1	°C
Ambient air pressure	1	bar
Pressure of Condenser	1	bar
Mass flow rate of air for each the condenser	1850	ton/hr
Condenser fans power for each level	520	kW
Re-injection Temperature Range	70-90	°C

* effectiveness of the heat exchangers are calculated by using real data of DORA-1 GPP.

6.1.2. Parametric Results

According to reservoir and ambient temperature of DORA-1 GPP, the Carnot efficiency is calculated 32.67%. The schematic layout of DORA-1 GPP is illustrated in Figure 6.1.

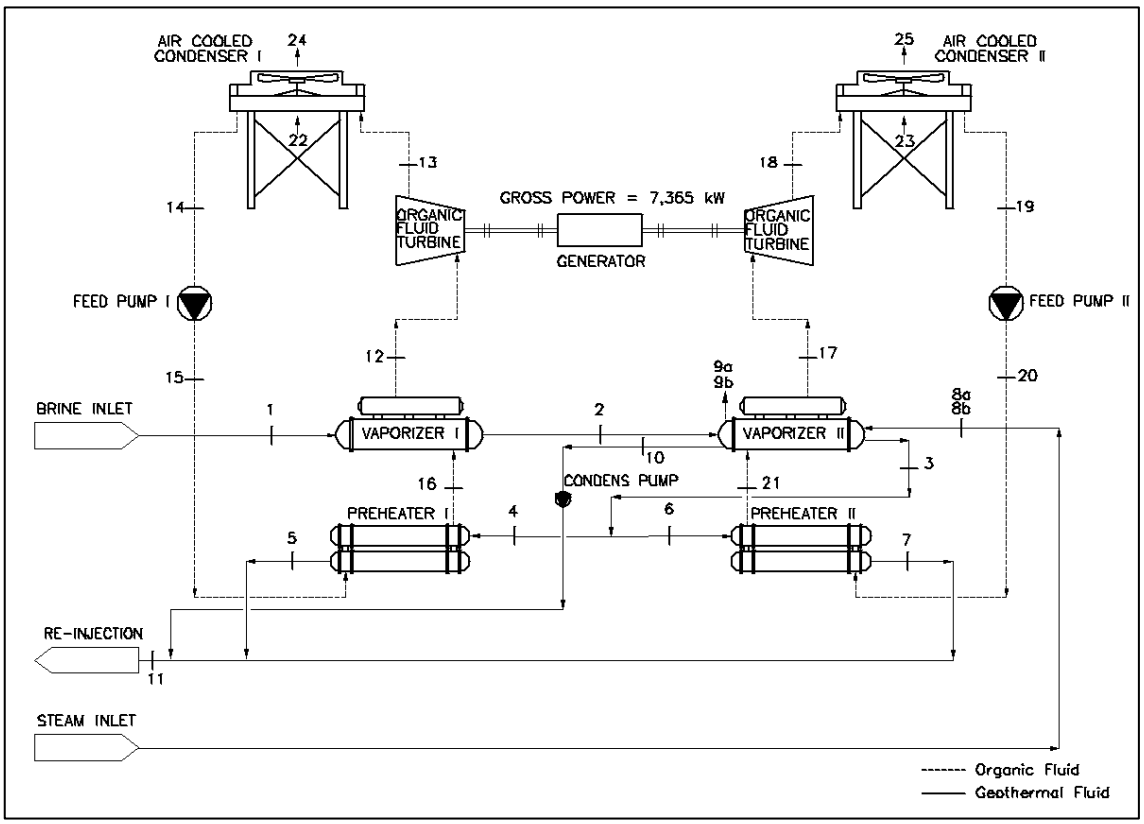

Figure 6.1. Schematic layout of DORA-1 GPP.

The brine, which is the heat source of the plant, firstly enters the vaporizer of Level 1 at 157.9 °C, heats the working fluid (n-pentane). Secondly, it enters the

vaporizer of Level 2 at 129.4 ^{0}C, and some heat of brine is transferred to the working fluid in this heat exchanger. Afterwards, the temperature of brine decreases to 112.1 ^{0}C and it divided equally to enter to the preheaters of Level 1 and 2. In preheaters 1 and 2, the brine temperatures a little more drop 84.04 and 79.51 ^{0}C, respectively. Finally, it is left from the power plant cycle and goes to reinjection wells. The vaporizer of Level 2 also has steam and NCG tube section. Steam and NCG pass through in this section at 150 ^{0}C, after that steam condenses and is pumped to reinjection pipe line by a condense pump at 109.2 ^{0}C.

Mass flow rate of working fluid is 56.13 kg/s, which circulates high pressure cycle, Level 1. N-pentane enters the preheater at 37.19 ^{0}C and leaves at 104.6 ^{0}C. After that, it enters the vaporizer and is evaporated at 133.1 ^{0}C. n-pentane then passes through the turbine and expands. Thus, this process brings about dropping in pressure and temperature as well as production of rotational shaft power by transforming kinetic energy gained by the vapors' expansion process. Working fluid exhaust at 81.39 ^{0}C and it condenses to temperature of 36.39 ^{0}C by an air cooled condenser which has 1850 kg/s mass flow rate of air at 17.1 ^{0}C. Finally, working fluid is pumped back into preheater by a feedpump and so Rankine cycle is completed. T-s and P-h diagram of Level 1 is shown in the Figure 6.2-6.3.

In Level 2, n-pentane circulates at 65.81 kg/s. It enters the preheater at 38.1 ^{0}C and leaves at 104.7 ^{0}C. It is heated until 109.1 ^{0}C in the vaporizer and then passes through the turbine. Working fluid enters the air cooled condenser at 70.8 ^{0}C and cooled until 37.51 ^{0}C. T-s and P-h diagram of Level 2 is shown in the Figure 6.4-6.5.

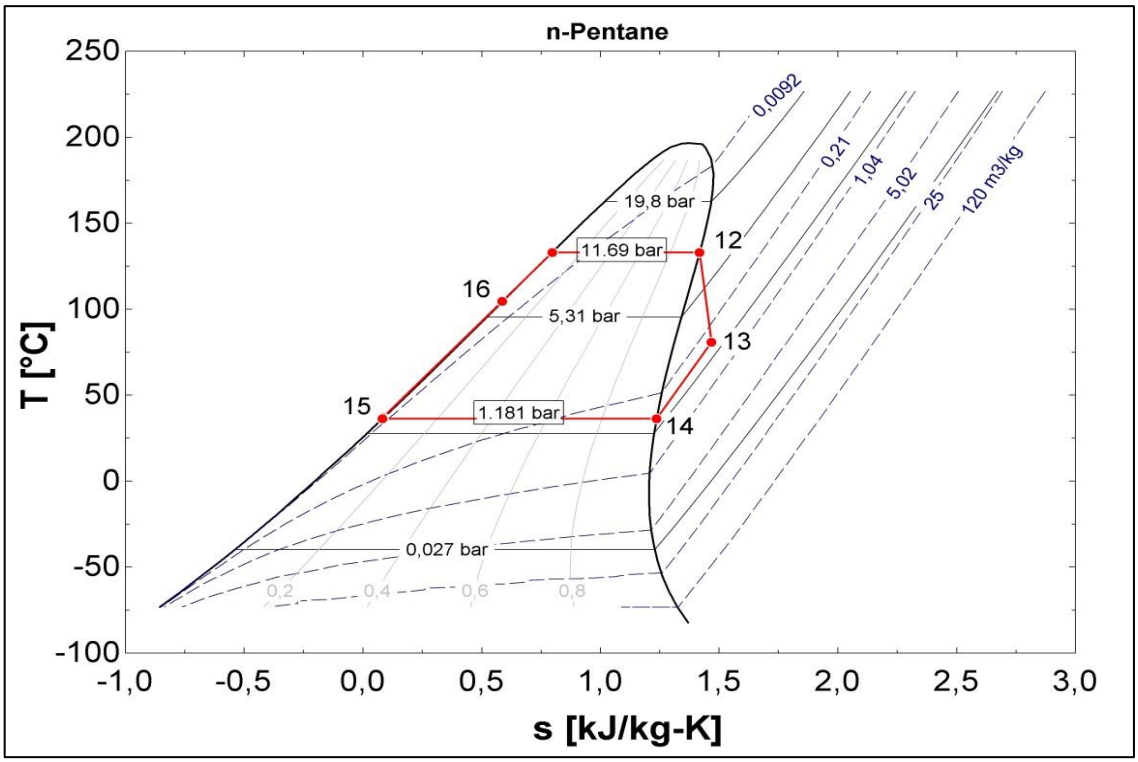

Figure 6.2. Temperature and entropy diagram of Level-1.

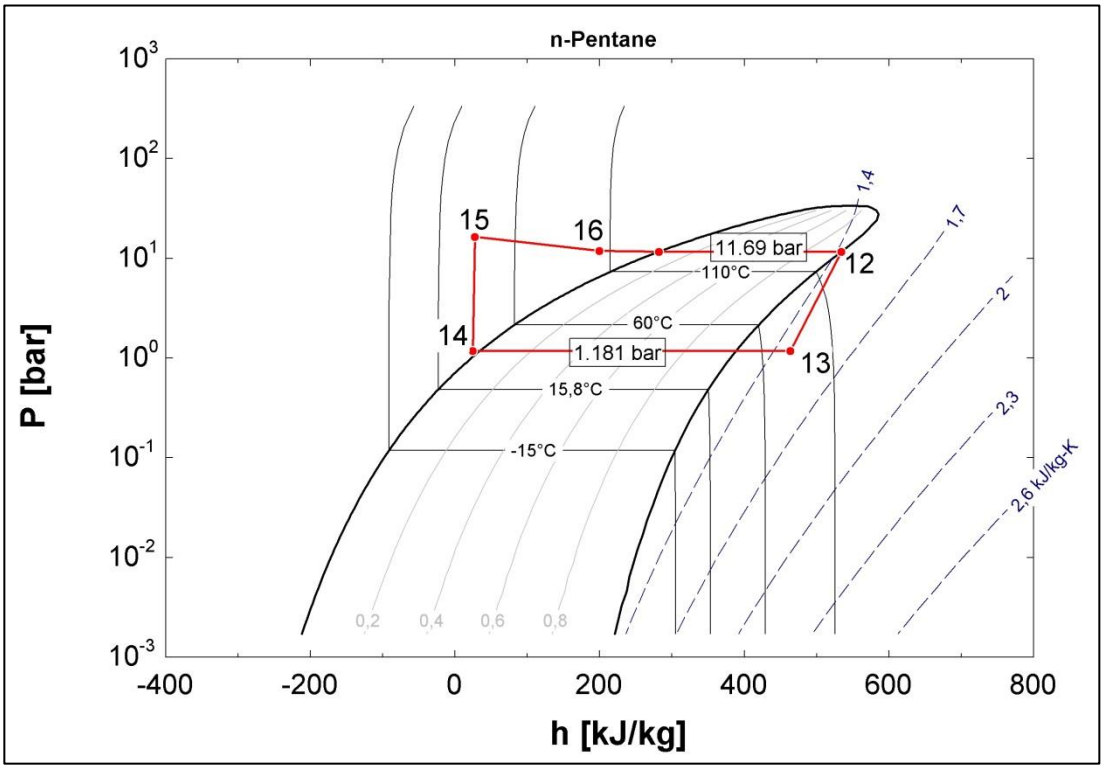

Figure 6.3. Pressure and enthalpy diagram of Level-1.

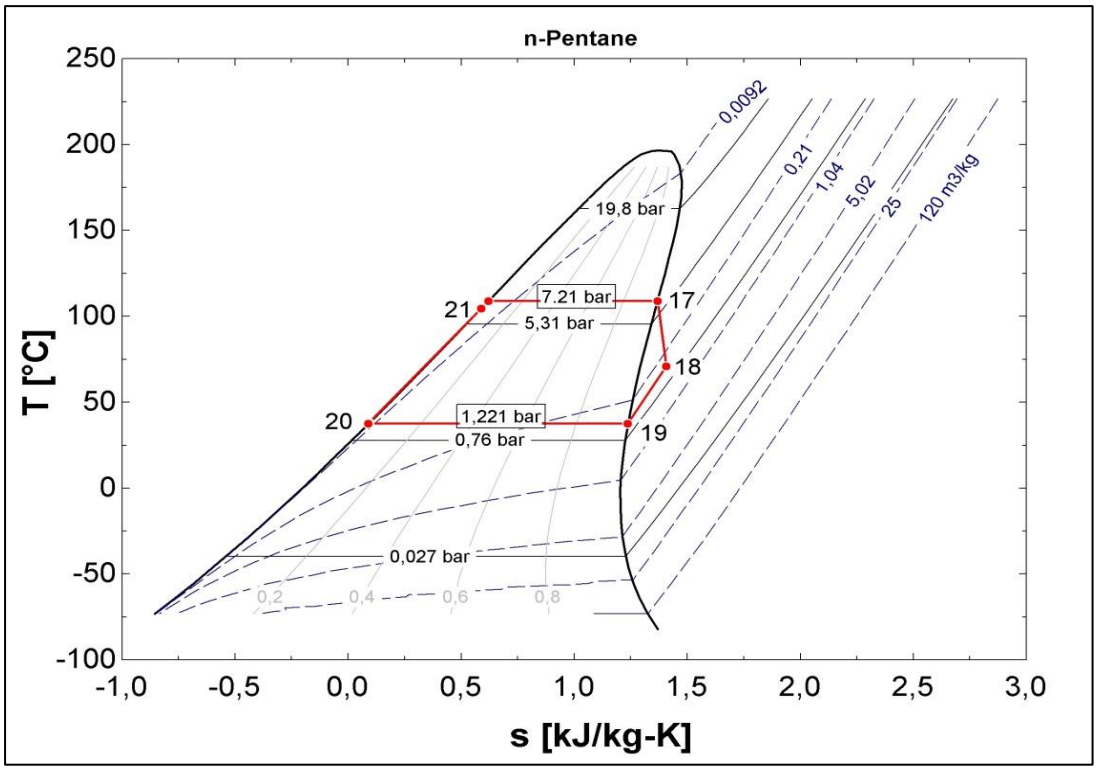

Figure 6.4. Temperature and entropy diagram of Level-2.

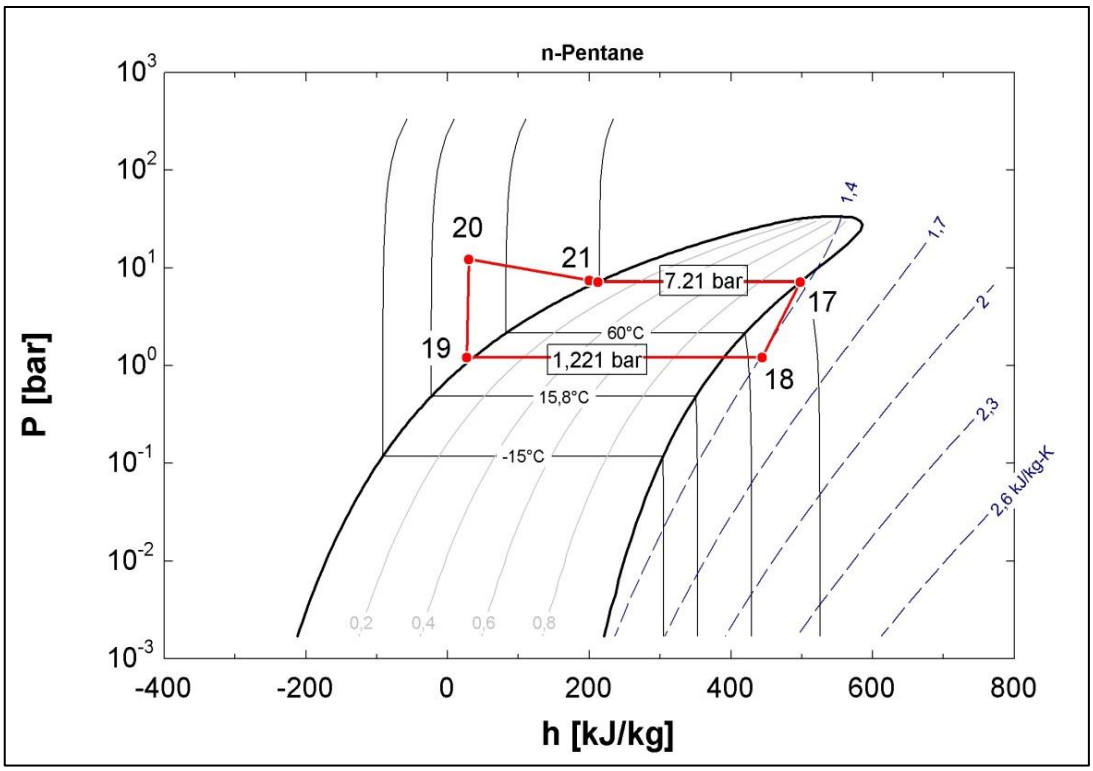

Figure 6.5. Pressure and enthalpy diagram of Level-2.

Figure 6.6 shows the heat transfer between brine and n-pentane for Level-1 high pressure cycle; Figure 6.7 shows the heat transfer between brine-steam-NCG and n-pentane for Level-2 low pressure cycle. Pinch point temperature of brine is 136.2 ^{0}C for Level-1 and 112.1 ^{0}C for Level-2. Pinch point temperatures which is simply the difference between brine pinch point temperature and vaporization temperature of n-pentane, 3.1 and 3 ^{0}C for Level-1 and 2, respectively.

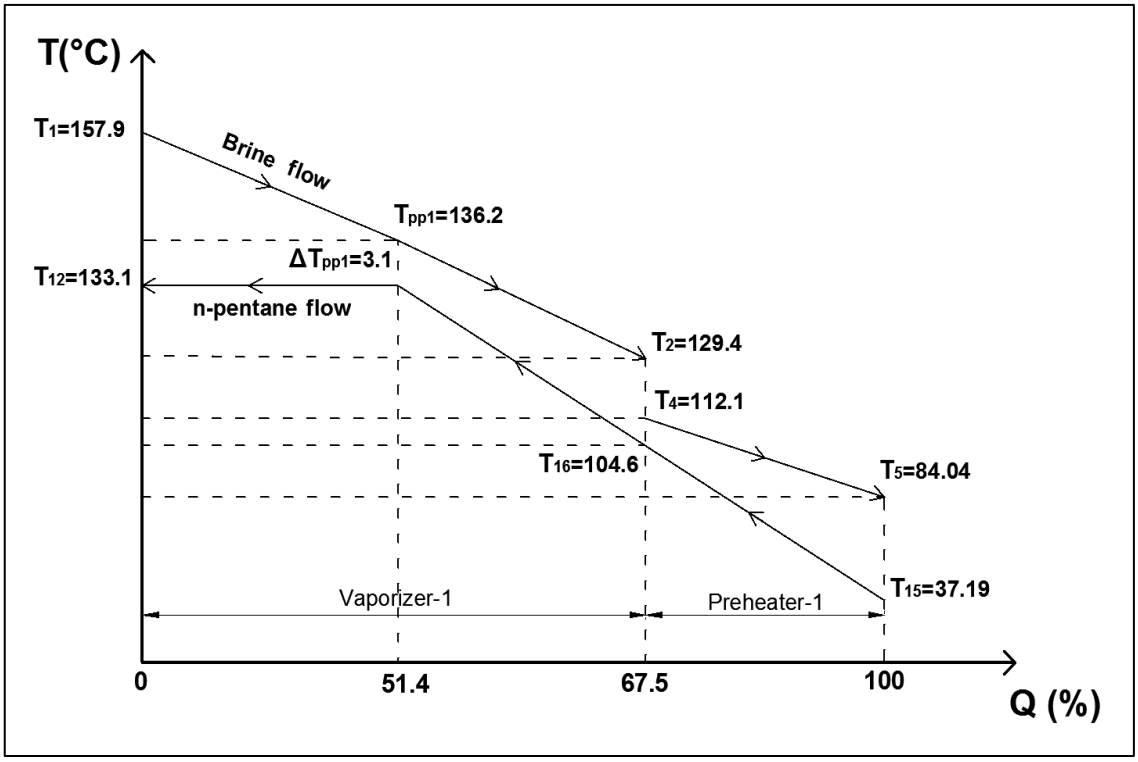

Figure 6.6. Temperature and heat diagram between geothermal fluid and n-pentane at Level-1.

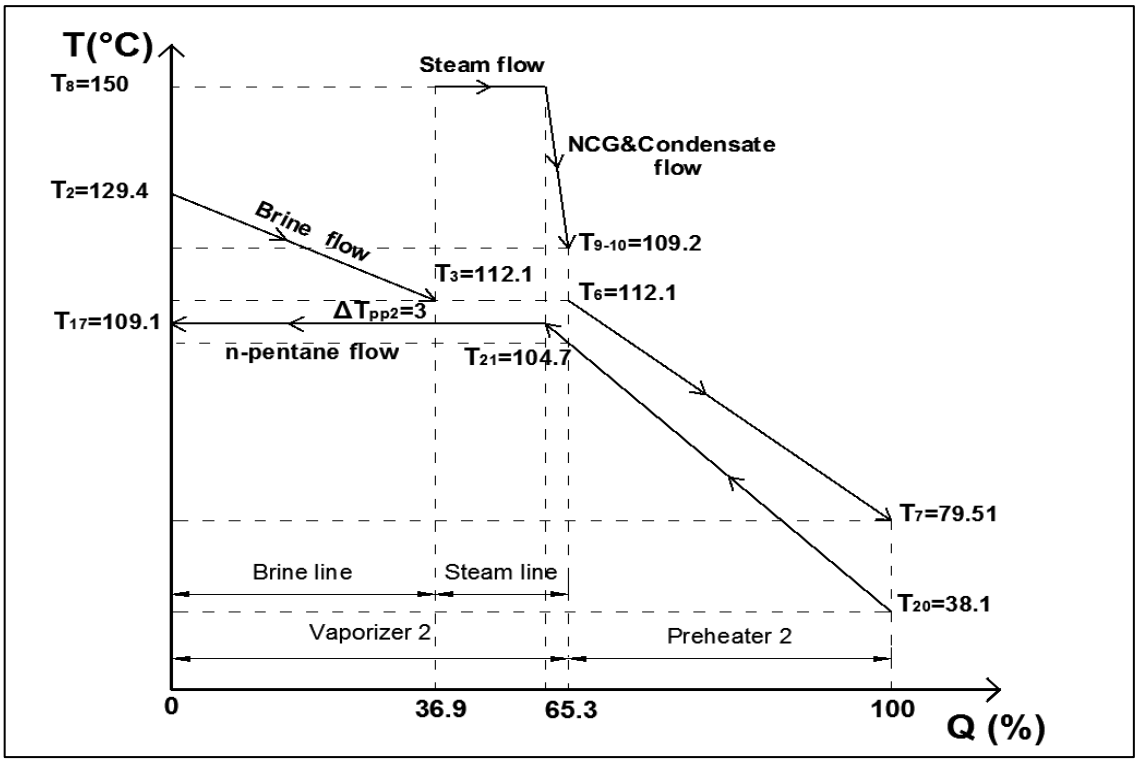

Figure 6.7. Temperature and heat diagram between geothermal fluid, steam&NCG and n-pentane at Level-2.

The thermodynamic properties of the DORA-1 GPP model state and energetic performance data of the power plant components are illustrated at Table 6.2 and 6.3

Table 6.2. Energetic performance data of the power plant components.

Component	Heat Transfer or Power (kW)	First Law efficiency (%)
Pump I	175,2	-
Preheater I	8953	-
Vaporizer I	18580	-
Turbine I	3937	-
Condenser I	24970	-
Pump II	149,8	-
Preheater II	10399	-
Vaporizer II	19588	-
Turbine II	3513	-
Condenser II	27629	-
Level I Cycle	27533	12.57
Level II Cycle	29987	10.2
Overall Plant	57520	11.32

Table 6.3. The thermodynamic properties of the DORA-1 GPP model state.

No	Description	Fluid	Phase	Pressure P(bar)	Temperature T(°C)	Enthalpy h(kj/kg)	Entropy s(kj/kgK)	Mass flow rate m(kg/s)
1	Vaporizer I inlet	Brine	Liquid	8	157,9	666,7	1,922	150,7
2	Vaporizer II inlet	Brine	Liquid	7,54	129,4	544	1,627	150,7
3	Vaporizer II outlet	Brine	Liquid	7,07	112,1	470,8	1,442	150,7
4	Preheater I inlet	Brine	Liquid	7,07	112,1	470,6	1,441	75,37
5	Preheater I outlet	Brine	Liquid	6,66	84,04	352,4	1,123	75,37
6	Preheater II inlet	Brine	Liquid	7,07	112,1	470,6	1,441	75,37
7	Preheater II outlet	Brine	Liquid	6,66	79,51	333,4	1,069	75,37
8a	Vaporizer II steam inlet	Steam	Vapor	5,7	150	2746	1,842	6,236
8b	Vaporizer II CO2 inlet	CO2	Vapor	5,7	150	110,4	-0,01557	2,095
9a	Vaporizer II unused steam outlet	Steam	Vapor	5,7	109,2	2960	7,247	0,4969
9b	Vaporizer II CO2 outlet	CO2	Vapor	5,7	109,2	71,43	-0,1124	2,095
10	Vaporizer II condense outlet	Brine	Liquid	5,7	109,2	458,4	1,41	3,644
11	Plant brine outlet	Brine	Liquid	6,637	82,43	345,6	1,104	154,4
12	Turbine I inlet	n-Pentane	Vapor	11,55	133,1	534,8	1,42	56,13
13	Turbine I outlet	n-Pentane	Vapor	1,181	81,39	464,7	1,47	56,13
14	Pump I inlet	n-Pentane	Liquid	1,181	36,39	24,6	0,08168	56,13
15	Pump I outlet	n-Pentane	Liquid	16,4	37,19	27,72	0,08366	56,13
16	Vaporizer I inlet	n-Pentane	Liquid	11,37	104,6	199,6	0,586	56,13
17	Turbine II inlet	n-Pentane	Vapor	7,52	109,1	497,5	1,368	65,81
18	Turbine II outlet	n-Pentane	Vapor	1,221	70,8	444,1	1,407	65,81
19	Pump II inlet	n-Pentane	Liquid	1,221	37,51	27,26	0,09023	65,81
20	Pump II outlet	n-Pentane	Liquid	12,3	38,1	29,54	0,09167	65,81
21	Vaporizer II inlet	n-Pentane	Liquid	7,5	104,7	199,8	0,5885	65,81
22	Condenser I inlet	Air	Gas	1	17,1	290,6	5,672	1850
23	Condenser II inlet	Air	Gas	1	17,1	290,6	5,672	1850
24	Condenser I outlet	Air	Gas	1	35,17	308,8	5,733	1850
25	Condenser II outlet	Air	Gas	1	37,38	311	5,74	1850

For these situations, turbine-1 and turbine-2 produce 3897.5 kW_e and 3469 kW_e electricity, respectively. Pump works are 175.2 kW_e and 149.8 kW_e for Level 1 and 2. Each condenser fans works are 520 kW_e and condense pump uses 7.5 kW_e electricity. Total net power production of plant is 6514 kW_e and thermal efficiency of plant is 12.37%.

6.1.3. Thermodynamic Performance Equations and Trends of the Plant

In this part, effects of parameter value changes are investigated to the plant performance and examined correlation between the net power production and the design parameters. Performance equations of DORA-1 GPP model are developed by using changing range of design parameters. Mathematical equations of the performance factors are shown below by change of each design conditions:

Table 6.4. The thermodynamic performance equations of the DORA-1 GPP model according to change of design parameters.

The changing parameters	Net Power Equation	Eqn. Number
Ambient air temp.	$\dot{W}_{net} = 7.563 - 0.0236\,T_{air} - 0.0027\,{T_{air}}^2 + 4E-5\,{T_{air}}^3$	(6.1)
Brine flow rate	$\dot{W}_{net} = -19.511 - 0.1364\,\dot{m}_{brine} - 0.0002\,{\dot{m}_{brine}}^2 + 2E-7\,{\dot{m}_{brine}}^3$	(6.2)
Brine temperature	$\dot{W}_{net} = -139{,}41 + 2.5542\,T_{brine} - 0.0152\,{T_{brine}}^2 + 3E-5\,{T_{brine}}^3$	(6.3)
Steam flow rate	$\dot{W}_{net} = 6.034 + 0.0001\,\dot{m}_{steam}\% + 8E-5\,\dot{m}_{steam}\%^2 - 3E-7\,\dot{m}_{steam}\%^3$	(6.4)
Steam NCG cont.	$\dot{W}_{net} = 7.6628 - 0.085\,\dot{m}_{NCG}\% + 0.0022\,\dot{m}_{NCG}\%^2 - 2E-5\,\dot{m}_{NCG}\%^3$	(6.5)

Net power is negatively correlated with ambient air temperature and NCG content of steam; positively correlated with brine temperature, mass flow rate of brine and steam. So, plant performance is increase by increasing of brine temperature, mass flow rates of brine and steam, decreasing of air temperature and NCG content of steam. Thermodynamic performance trends of the DORA-1 GPP model are displayed in Figures 6.7-6.11.

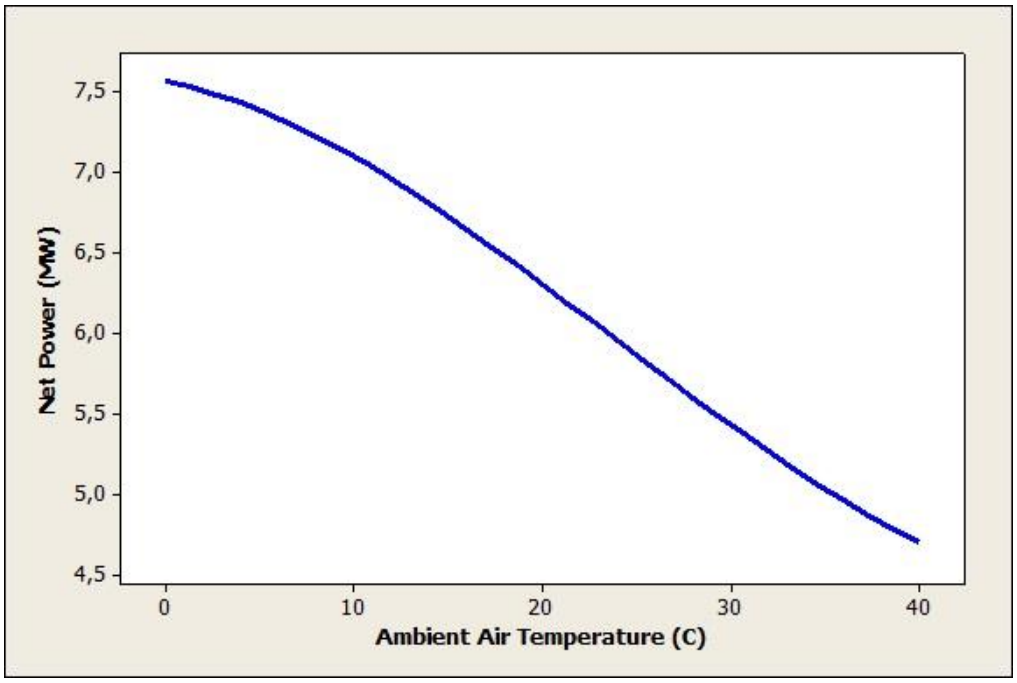

Figure 6.7. Net power generation trend by changing ambient air temperature.

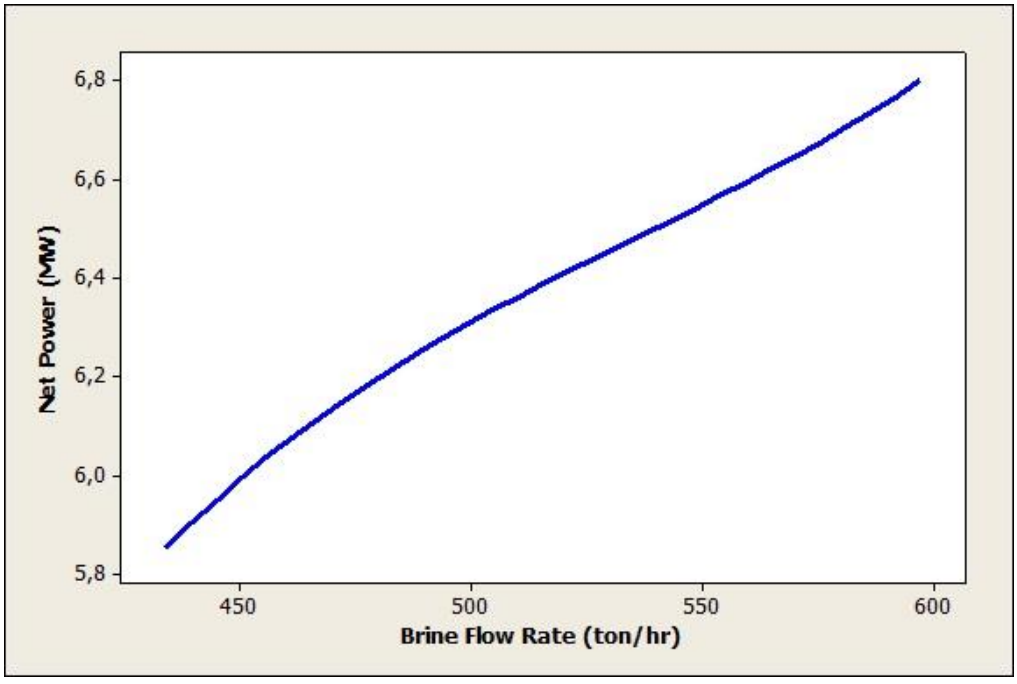

Figure 6.8. Net power generation trend by changing brine flow rate.

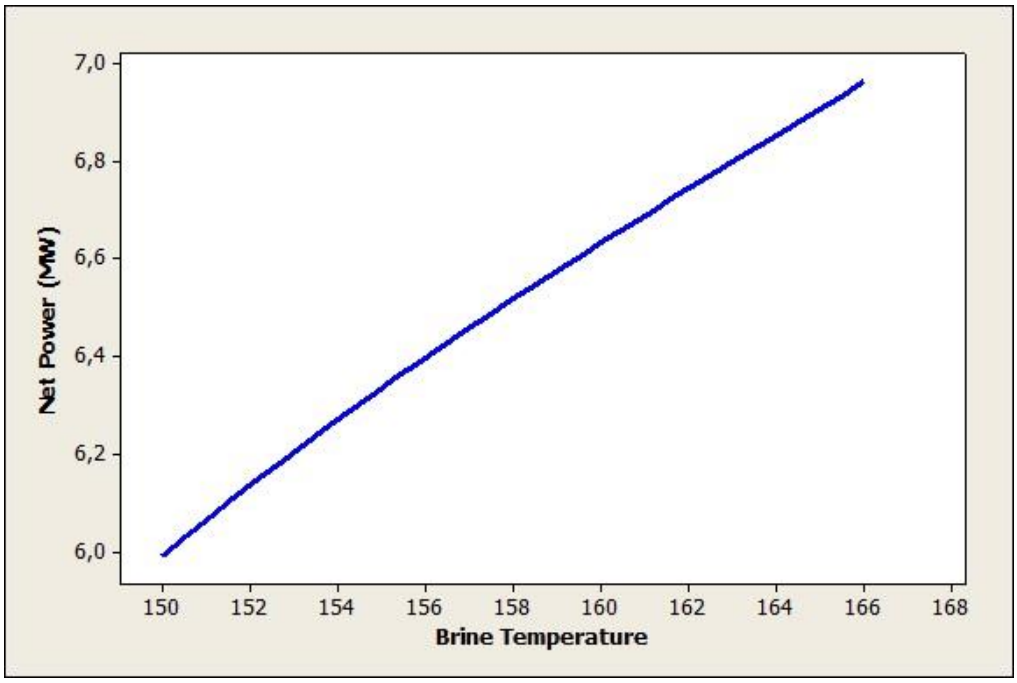

Figure 6.9. Net power generation trend by changing brine temperature.

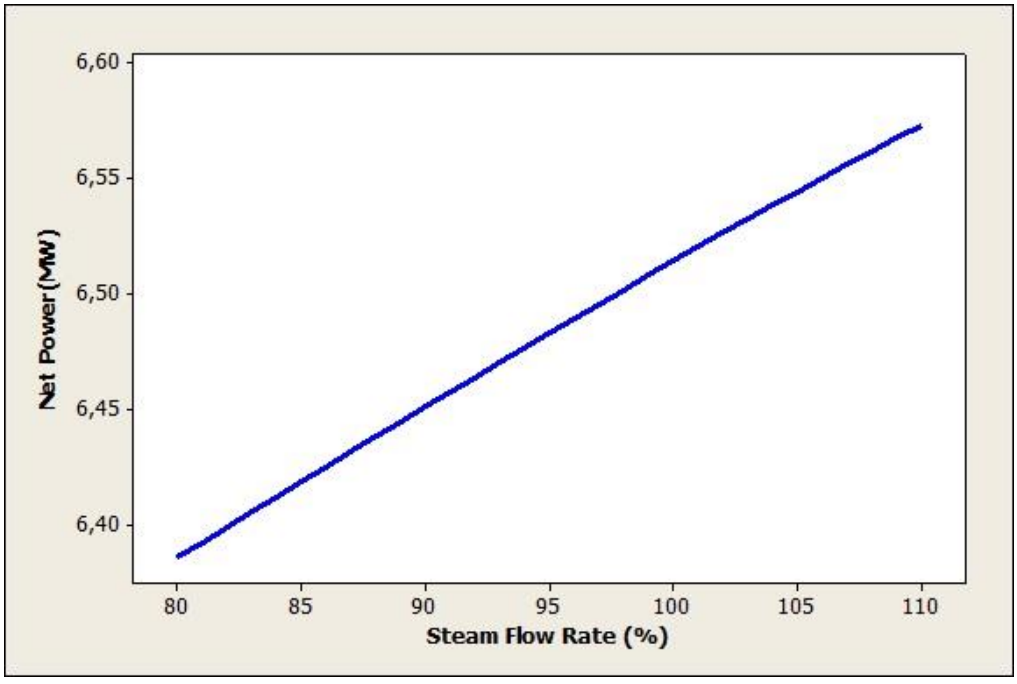

Figure 6.10. Net power generation trend by changing steam flow rate.

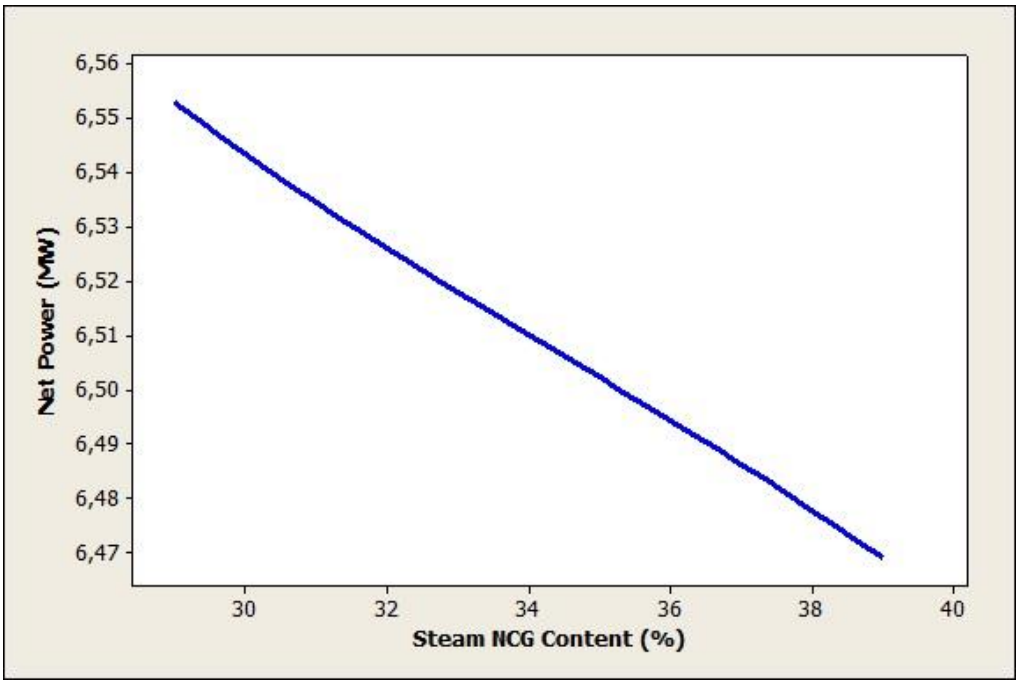

Figure 6.11. Net power generation trend by changing steam NCG content.

6.2. Regression Model

This part investigates multiple linear regression analysis of DORA-1 GPP, using the annual plant data from 2006 to 2012 and the annual performance models of DORA-1 GPP are developed. First, regression model of DORA-1 GPP is built for plant data of 2010 and the assumptions of classical linear regression model are applied for this model. After that, the same procedure is applied to the annual plant data. This parametric study of the power plant behavior with the ambient air temperature, geothermal fluid (brine) temperature and brine mass flow rate are also evaluated by using the validated power plant performance model.

6.2.1. Data

The data, which were eliminated due to breakdown of the plant, is hourly gathered from DORA-1 GPP in Aydın. All parameters are measured on DORA-1 GPP from 2006 to 2012 and the models are built by using 49411 hourly time series data. Performance of power plant (Net power) depends on five parameters. These are ambient

air temperature, brine temperature, brine mass flow rate, NCGs and steam mass flow rate.

Table 6.5. Minimum, maximum, mean and standard deviation of variables of DORA-1

Measuring Variables in 2010						
Group	Variables	Unit	For the 8412 inputs			
			Min.	Max.	Mean	Std. Deviation
Dependent	Net Power	MW	3,19	7,60	5,94	0,943
Independent	Ambient Air Temperature	°C	0	42,70	19,91	8,16
	Brine Inlet Temperature	°C	157,04	159,98	158,51	0,49
	Total Brine Flow Rate	ton/hour	483,00	601,00	546,17	27,57

DORA-1 reported a problem related to a mismeasurement of steam and NCG mass flow rates. The effects of these parameters were very low in that steam and NCG mass flow rates are theoretically at 4% level of total mass flow rate. Since the mass flow rates of these variables were not correctly measured, they were not used in the present study, which caused an increase in error term.

Consequently, only the effects of the ambient air temperature, the brine mass flow rate and the brine temperature have been examined to net power. Minimum, maximum, mean and standard deviation of all measured real data for 2010 is shown in Table 6.5.

6.2.2. Estimations and Results for Time Series Data of 2010

In this part, linear and non-linear models were built, tested and compared by using all independent variables. The data were analyzed by a statistical package programme (SPSS 17.0). The dependent variable was the net power production and the independent variables were the ambient air temperature, the brine temperature and brine mass flow rate which was a controlled variable. The variables were analyzed by the repeated measures over time.

Normality of each individual variable with the dependent variable was analyzed by Kurtosis and Skewness tests (Table 6.6). The scatterplots of independent variables are shown in Figure 2. The square of the ambient air temperature was also added to the

linear forecasting model as an independent variable because the upper tail of the ambient air temperature distribution seems quadratic (Figure 6.12a).

Table 6.6. Skewness and Kurtosis values of the independent variables

Independent Variables	Skewness	Kurtosis
Ambient Air Temperature	0.208	-0.512
Brine Flow Rate	-0.405	-1.310
Brine Temperature	-0.44	-0.101
Ambient Air Temperature Square	1	0.409

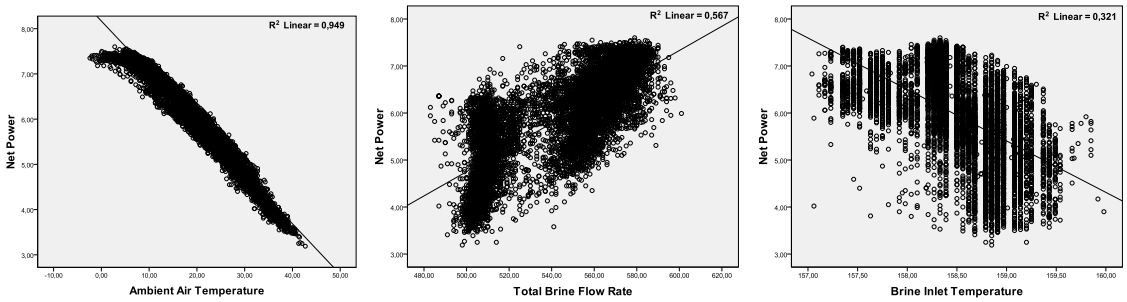

a b c

Figure 6.12. Relationships between dependent variable and independent variables

All the independent variables except for brine flow rate satisfy normality due to Skewness and Kurtosis tests. The Kurtosis test result of the brine flow rate, which should be between -1.0 and +1.0, is outside the range of normality. When the scatter plot of brine mass flow rate is investigated, the distribution of the brine mass flow rate is mainly gathered in two areas (Figure 6.12b). This situation is caused by operation conditions of the plant. If the two areas are examined, both regions separately show normal distributions. Therefore, the brine mass flow rate provides normality assumption and transformation is not necessary for the brine mass flow rate.

The inputs and equations of the two models are presented in Table 6.7. In the first model, all coefficients of independent variables are linearly used while parameters of the second model are non-linear. Nevertheless, the second model is parametrically linearized to test the assumptions of classical linear regression.

Table 6.7. The inputs and equations of the two models

Model	Inputs	Equations	Equation Number
1. Linear	$X_1, X_2, X_3, {X_1}^2$	$\hat{Y} = b_0 + b_1X_1 + b_2X_2 + b_3X_3 + b_4{X_1}^2$	(6.6)
2. Non-linear	X_1, X_2, X_3	$\hat{Y} = b_0{X_1}^{b_1}{X_2}^{b_2}{X_3}^{b_3}$	(6.7)

Preliminary results of the regression models are shown in Table 6.8. The structure of hypothesis testing for these models can be built to control F-testing as follows:

H_0: $b_1 = b_2 = b_3 = b_4 = 0$

H_A: $b_i \neq 0$ (at least one)

According to the null hypothesis, none of the independent variables is significantly related to the dependent variable. But an alternative hypothesis is that at least one of the independent variable is significantly related to the dependent variable. F-test and t-test results of independent variables for the two models are also shown in Table 6.8. The null hypothesis is rejected for both models because F-test results are found to be significant according to the ρ-value ($\rho < 0.05$). At the $\alpha = 0.05$ level of significance, there exists enough evidence to conclude that predictors are useful for predicting net power; therefore both of the models are useful.

Table 6.8. Statistical details and equations for each regression model

Model	Equation					Eqn. Number
1. Linear	$\hat{Y} = b_0 + b_1T_{air} + b_2\dot{m}_{brine} + b_3T_{brine} + b_4{T_{air}}^2$					(6.8)
	$R^2 = 0.992$ $\quad F-test = 125398.43, \rho = 0$					
	oefficients	b_0 =1.976	b_1=-0.053	$b_2 = 0.008$	$b_3 = 0.007$	$b_4 = -0.001$
	t-statistics	$t = 3.783$	$t = -74.52$	$t = 146.12$	$t = 2.121$	$t = -61.46$
		$\rho < 0.05$	$\rho < 0.05$	$\rho < 0.05$	$\rho < 0.05$	$\rho < 0.05$
			VIF = 20.4	VIF = 1.68	VIF = 1.519	VIF = 19.75
2. Non-linear	$\ln\hat{Y} = \ln b_0 + b_1 \ln T_{air} + b_2 \ln\dot{m}_{brine} + b_3 \ln T_{brine}$					(6.9)
	$R^2 = 0.818$ $\quad F-test = 12620.432, \rho = 0$					
	Coefficients	$b_0' = 26.91$	$b_1 = -0.178$	$b_2 = 1.366$	$b_3 = -6.561$	
	t-statistics	$t = 17.32$	$t = -89.508$	$t = 73.846$	$t = -21.631$	
		$\rho = 0 < 0.05$	$\rho = 0 < 0.05$	$\rho = 0 < 0.05$	$\rho = 0 < 0.05$	
			VIF = 1.693	VIF = 1.429	VIF = 1.399	

According to t-test results of independent variable coefficients, all controlled variables are significant at α=0.05 level of significance. VIF values of the ambient air temperature and its square in the first model are 20.4 and 19.75, respectively. These results indicate that there is multicollinearity between the two variable, which is an expected finding because one is the square of the other one. VIF of the brine mass flow rate and brine temperature are less than 5 in linear model. Therefore, there is not multicollinearity between the independent variables of linear model. On the other hand, multicollinearity is not found among the independent variables in the non-linear model. Equation of the relevant models, which are significant as coefficient for t-test, consisted in Table 6.9.

Table 6.9. Equations of useful models

Model	Equations	Eqn. Numb.
1. Linear	$\hat{Y} = 1.196 - 0.053T_{air} + 0.008\dot{m}_{brine} + 0.007T_{brine} - 0.001{T_{air}}^2$	(6.10)
2. Non-linear	$\ln\hat{Y} = 26.910 - 0.178\ln T_{air} + 1.366\ln\dot{m}_{brine} - 6.561\ln T_{brine}$	(6.11)

Coefficients of determination of the linear and non-linear models are respectively 0.992 and 0.818 (Table 6.10). It can be seen that the linear model gives a better fit than the non-linear model. However, this information is not enough to decide which model is the best. Important properties about estimation of the models are compared in Table 6.10. The coefficient of variation and the standard error of estimate of the non-linear regression model are slightly lower than the linear regression model. Additionally, there are positive serial autocorrelation between the errors for both models because Durbin-Watson statistic results are lower than 2.

Table 6.10. Mean, standard error, coefficient of variation, Durbin-Watson statistics results and coefficients of determination values of the estimates

Model	Mean of estimate	Std. error of estimate	Coefficient of variation	Durbin-Watson Statictics (d)	R^2
1. Linear	5.94	0.101	0.0218	0.929	0.992
2. Non-linear	5.942	0.0725	0.0169	0.212	0.818

The regression analysis should be reapplied to both models by using Orcutt-Cochran method to eliminate autocorrelation. The Orcutt-Cochran regression results for two models are displayed in Table 6.11.

Table 6.11. Final models are obtained by Orcutt-Cochran method

Model	Regression Equations	Durbin-Watson Statictics (d)	R^2	Eqn. Numb.
1. Linear	$\hat{Y} = 1.506 - 0.053T_{air} + 0.007\dot{m}_{brine} - 0.013T_{brine} - 0.001{T_{air}}^2$	2.213	0.946	(6.12)
2. Non-linear	$\ln\hat{Y} = -2.62 - 0.121\ \ln T_{air} + 0.751\ \ln\dot{m}_{brine}$	1.661	0.435	(6.13)

According to Orcutt-Cochran test results, the brine temperature is removed in non-linear model because the parameter of the brine temperature is insignificant at the α=0.05 level of significance. Durbin-Watson statistics value increased from 0.929 to 2.213 after 3 iterations by Orcutt-Cochran method and the coefficient of determination decreased from 0.992 to 0.946 for the linear model. For the non-linear model, Durbin-Watson test value increased from 0.212 to 1.661 after 4 iterations while the coefficient of determination decreased from 0.818 to 0.435.

Although errors of linear model include negative serial autocorrelation, Durbin-Watson statistics result of linear model is the closest to the 2 than non-linear model. Also, the linear model fits better than the non-linear model in Orcutt-Cochran regression. The results of these tests show that linear model is the best estimation of regression for net power production. The regression equation is correctly specified in following equation for year 2010.

$$\hat{Y} = 1.506 - 0.053T_{air} + 0.007\dot{m}_{brine} - 0.013T_{brine} - 0.001{T_{air}}^2 \qquad (6.14)$$

6.2.3. Annual and Perennial Regression Analysis of DORA-1 GPP

DORA-1 GPP is installed in May 2006 and all performance data of plant have been recorded since September 2006 by GEOPERFORM, which is a software programme (Gülgezen et al., 2007). Annual regression models are created by using data collected in GEOPERFORM to find statistical performance equations of the plant and to investigate annual performance change of the plant.

Steam and NCG flow rates were not included in the models because they were not correctly measured on the plant. During the regression analysis, the brine temperature was not significant according to t-statistics for each year. So, all regression models were created with mass flow rate of the brine and the ambient air temperature. The positive serial autocorrelation was the main problem of the annual regression models. Models were eliminated from the autocorrelation by Orcutt-Cochran regression.

Annual performance models per 1˚C change in ambient air temperature at design conditions are illustrated in Figure 6.13 and the annual regression equations are presented at Table 6.12.

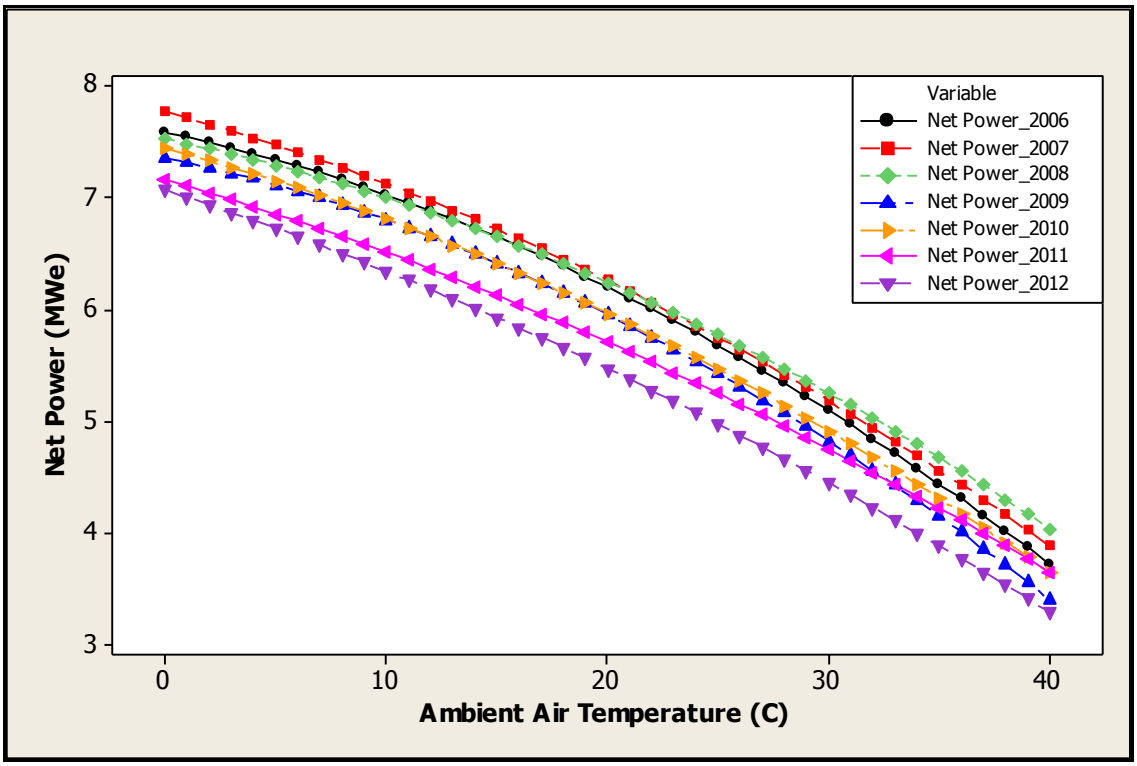

Figure 6.13. Annual performance models per 1˚C change in ambient air temperature at design conditions (at 542.65 tons/hour brine flow and 157.9˚C brine temperature)

Table 6.12. Annual regression models of Dora-1

Years	Annual Regression Equations	Durbin-Watson Statictics (d)	R^2	Eqn.
2006	$\hat{Y} = 2.705 - 0.042T_{air} + 0.009\dot{m}_{brine} - 0.001{T_{air}}^2$	2.052	0.88	(6.15)
2007	$\hat{Y} = -1.422 - 0.054T_{air} + 0.006\dot{m}_{brine} - 0.039T_{brine} - 0.001{T_{air}}^2$	2.189	0.94	(6.16)
2008	$\hat{Y} = -0.84 - 0.041T_{air} + 0.007\dot{m}_{brine} - 0.028T_{brine} - 0.001{T_{air}}^2$	2.478	0.87	(6.17)
2009	$\hat{Y} = -26.536 - 0.041T_{air} + 0.005\dot{m}_{brine} - 0.197T_{brine} - 0.001{T_{air}}^2$	2.084	0.93	(6.18)
2010	$\hat{Y} = 1.506 - 0.053T_{air} + 0.007\dot{m}_{brine} - 0.013T_{brine} - 0.001{T_{air}}^2$	2.213	0.94	(6.19)
2011	$\hat{Y} = -4.619 - 0.058T_{air} + 0.005\dot{m}_{brine} - 0.057T_{brine} - 0.001{T_{air}}^2$	2.588	0.67	(6.20)
2012	$\hat{Y} = -27.361 - 0.065T_{air} + 0.008\dot{m}_{brine} - 0.192T_{brine} - 0.001{T_{air}}^2$	2.717	0.78	(6.21)

According to annual regression models, the performance models of the plant from 2006 to 2008 are very close. As can be seen in the Figure 6.13, degradation of plant performance especially started by 270 kWe decreasing from 2009 to 2010 years. Annual multiple regression analysis shows that the performance of the plant decreased 550 kWe in 2011 and total degradation of plant performance reached to 760 kWe according to design conditions by 2012.

6.2.4. Regression Performance Equations and Trends of the Plant

Performance equations of DORA-1 GPP according to changing of ambient air temperature, brine flow rate and brine temperature for 2008 year are shown in Table 6.13. Their trends are also illustrated in Figure- 6.14-6.16.

Table 6.13. The performance equations of the DORA-1 GPP regression model (2008 year) according to change of design parameters.

The variable parameters	Net Power Equation	Eqn. Number
Ambient air temp.	$\dot{W}_{net} = 7.5267 - 0.0411\,T_{air} - 0.0012\,{T_{air}}^2 - 7E-18\,{T_{air}}^3$	(6.22)
Brine flow rate	$\dot{W}_{net} = 2.5821 + 0.039\,\dot{m}_{brine} + 6E-15\,{\dot{m}_{brine}}^2 - 3E-17\,{\dot{m}_{brine}}^3$	(6.23)
Brine temperature	$\dot{W}_{net} = 2.0236 + 0.0283\,T_{brine} + 6E-14\,{T_{brine}}^2 - 1E-16\,{T_{brine}}^3$	(6.24)

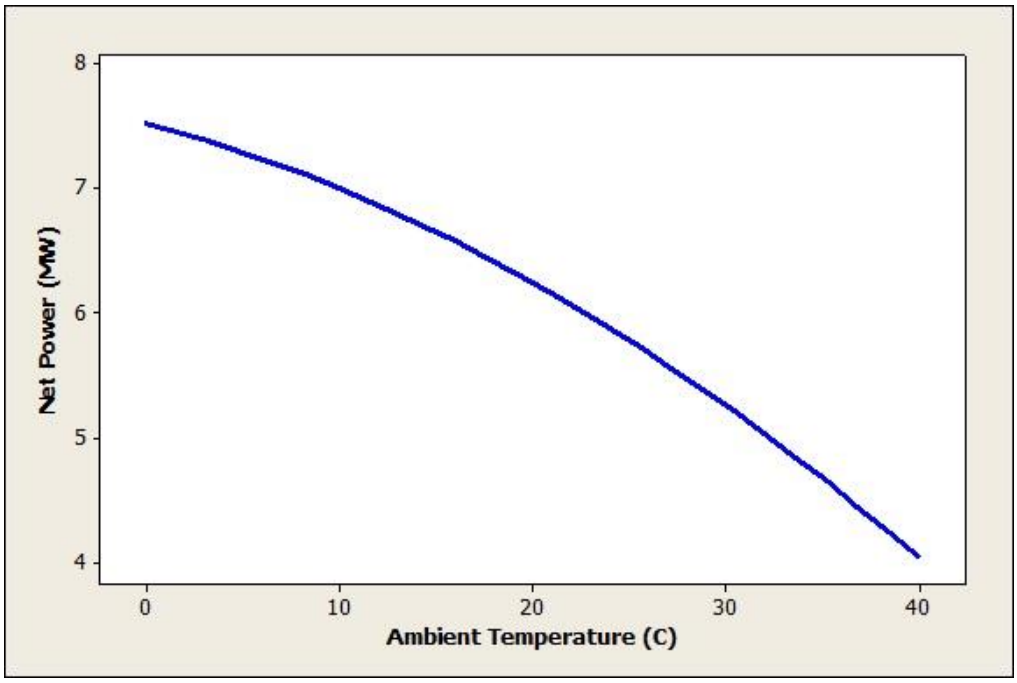

Figure 6.14. Net power generation by changing ambient temperature.

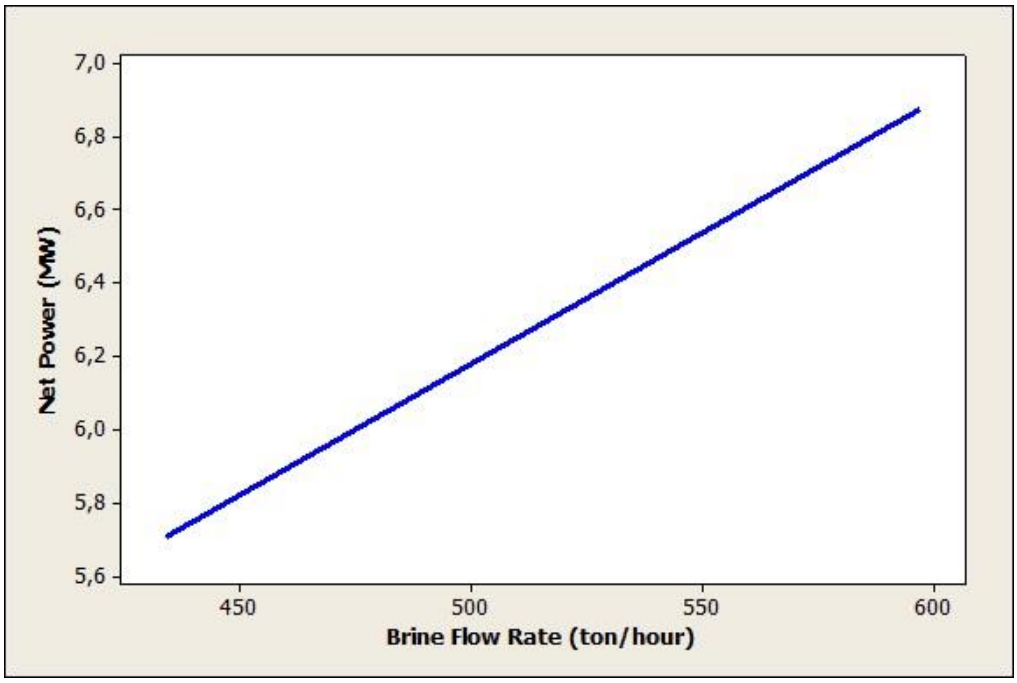

Figure 6.15. Net power generation by changing brine flow rate.

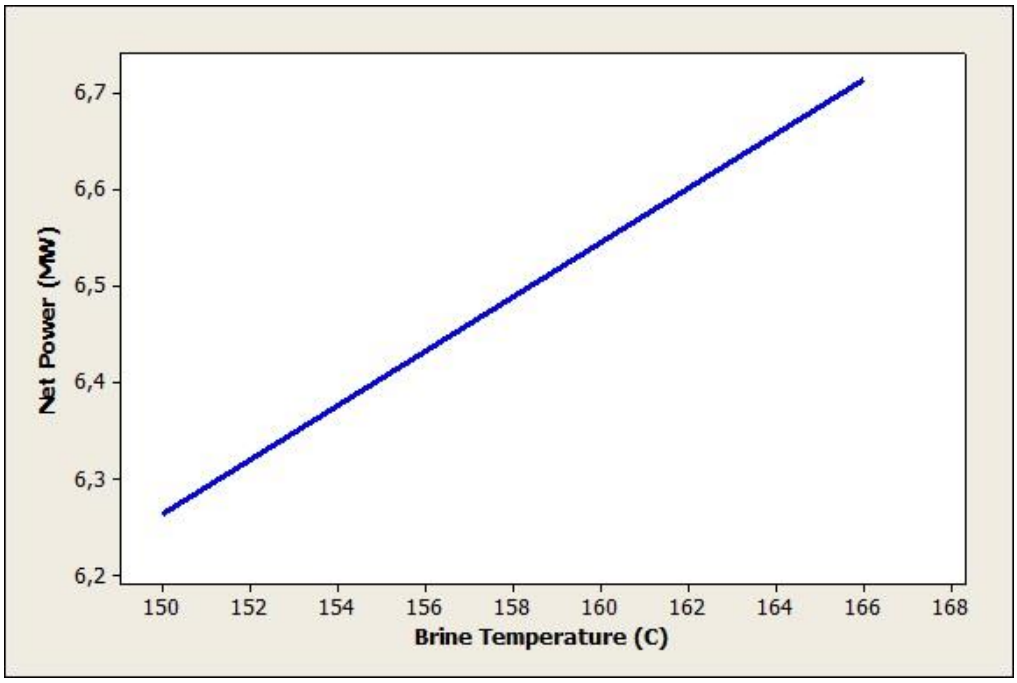

Figure 6.16. Net power generation by changing brine temperature.

6.3. Comparison of Theoretical, Regression and Ormat Net Power Correction Factors

The theoretical net power correction factors are computerized as polynomial functions by using thermodynamic model of DORA-1 GPP for all design parameters. The regression net power correction factors are also built by using regression analysis of DORA-1 GPP according to the plant data of 2008 year for only the ambient air temperature, the brine flow rate and the brine temperature variables. The equations of the net power correction factors are given in Table 6.14 and 6.15.

Table 6.14. The theoretical net power correction factors.

The variable parameters	Net Power Equation	Eqn. Number
Ambient air temperature	$F1 = 1.15 - 0.001\,T_{air} - 0.0006\,{T_{air}}^2 + 8E-6\,{T_{air}}^3$	(6.25)
Steam flow rate	$F2 = 0.712 + 0.046\,\dot{m}_{steam}\% - 2E-5\,\dot{m}_{steam}\%^2$	(6.26)
Steam NCG content	$F3 = 1.008 - 0.0001\,\dot{m}_{steam}\% - 4E-6\,\dot{m}_{steam}\%^2$	(6.27)
Brine flow rate	$F4 = -2.9952 + 0.1136\,\dot{m}_{brine} - 0.0011\,{\dot{m}_{brine}}^2 + 4E-6\,{\dot{m}_{brine}}^3$	(6.28)
Brine temperature	$F5 = -8.062 + 0.102\,T_{brine} - 0.0002\,{T_{brine}}^2 - 2E-7\,{T_{brine}}^3$	(6.29)

Table 6.15. The net power correction factors of the DORA-1 GPP regression model (2008 year) according to change of design parameters.

The changing parameters	Net Power Equation	Eqn. Number
Ambient air temperature	$F1 = 1.1604 - 0.0063\,T_{air} - 0.0002\,{T_{air}}^2 - 2E-18\,{T_{air}}^3$	(6.30)
Brine flow rate	$F4 = 0.3981 + 0.006\,\dot{m}_{brine} + 2E-15\,{\dot{m}_{brine}}^2 - 1E-17\,{\dot{m}_{brine}}^3$	(6.31)
Brine temperature	$F5 = 0.312 + 0.0044\,T_{brine} - 2E-14\,{T_{brine}}^2 + 4E-17\,{T_{brine}}^3$	(6.32)

The comparison of theoretical, regression and Ormat net power correction factors are illustrated from Figure 6.17 to 6.21.

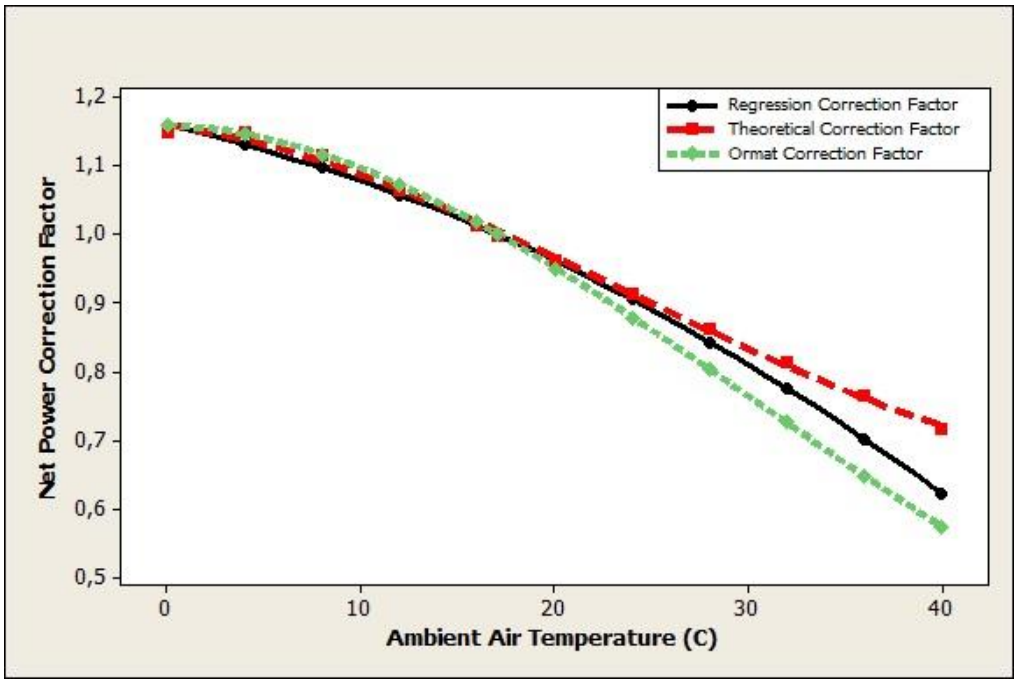

Figure 6.17. Net power generation by changing brine temperature.

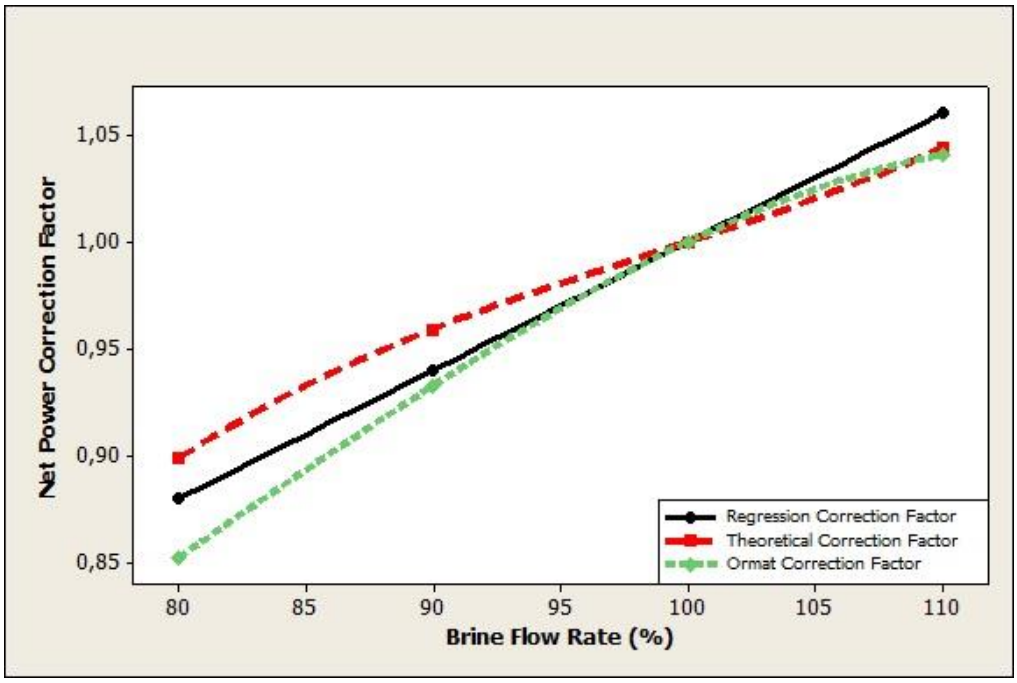

Figure 6.18. Net power generation by changing brine flow rate.

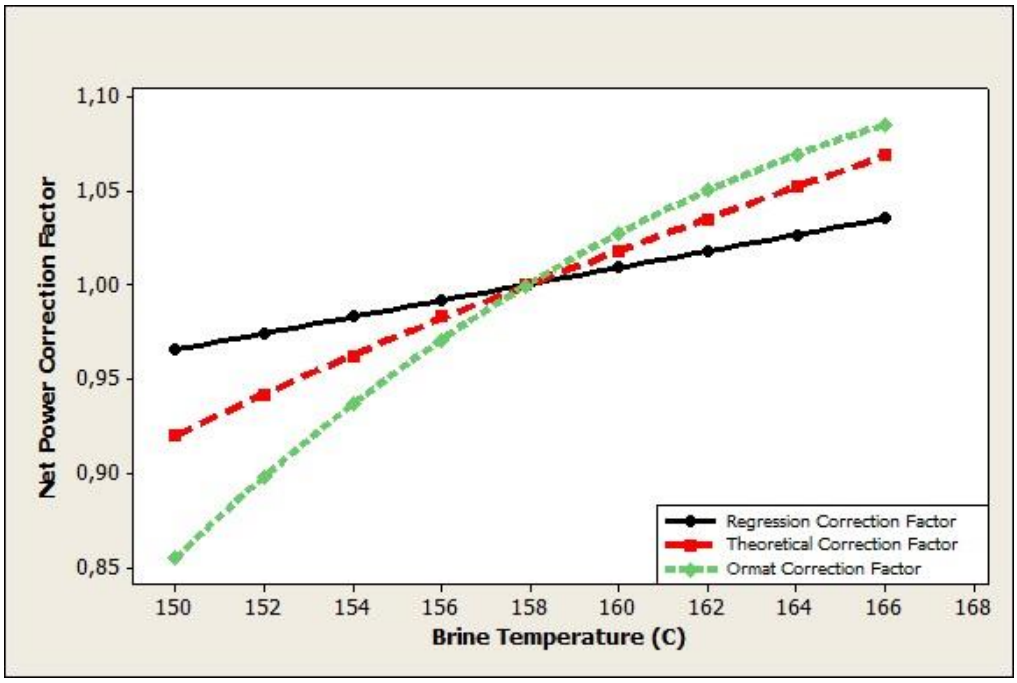

Figure 6.19. Net power generation by changing brine temperature.

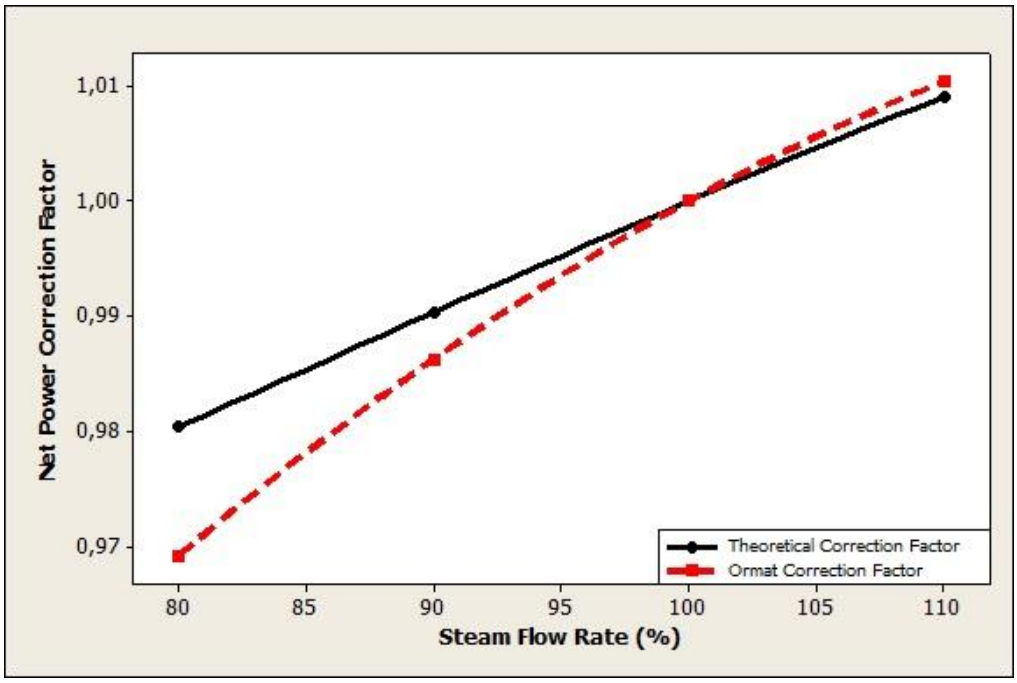

Figure 6.20. Net power generation by changing brine temperature.

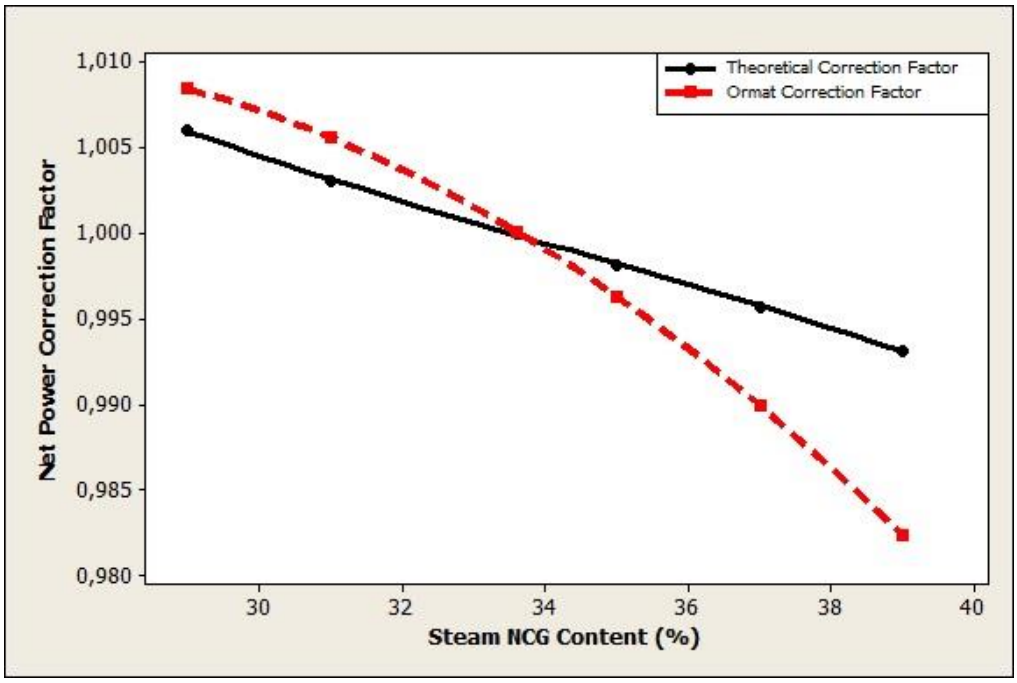

Figure 6.21. Net power generation by changing brine temperature.

CHAPTER 7

CONCLUSIONS

A deterministic model of an air cooled binary cycle GPP is developed using real reservoir and ambient data of DORA-1 GPP and a code written EES software. Besides, statistic models of DORA-1 GPP are performed by regression analysis to assess the performance status of the plant and calculated real performance equations using actual plant data. The theoretical and regression performance equations are compared with Ormat performance models.

- **Thermodynamic model**
    - The thermal efficiency of the theoretical plant is calculated 11.32 % at 157.9 ^{0}C geothermal resource and 17.1 ^{0}C ambient air conditions. Efficiency of the plant increases with increasing the source temperature and decreasing the sink temperature.
    - The performance equations of the theoretical plant are identified for changing of five design parameters: ambient air temperature, brine flow rate ad temperature, steam flow rate and NCG content.
    - After that, the polynomial functions of the net power correction factors are calculated for theoretical model. According to this model, the net power generation of the plant increases with an increase in brine temperature, and mass flow rates of brine and steam; decreases with an increase of ambient air temperature and NCGs content of the steam. Ambient air temperature is the most effective parameter on electricity generation, because the efficiency of a plant mainly depends on the difference between the temperatures of the source (geothermal fluid) and the sink (air).

- **Regression model**
    - The regression modeling part of the Thesis, which is the first study about estimated of performance status of a geothermal power plant, used a

comprehensive multiple linear regression analysis in order to investigate the annual performance of a binary geothermal power plant in Turkey.

- In multiple linear regression analysis, the linear and the non-linear models are built for a year by using time series data of 3 measured independent variables: the ambient air temperature, the brine temperature and the mass flow rate. The aim of these models is to develop a function of the plant performance estimation for a geothermal power plant which depends on interpretability, clarity and easy to use. The parameter of the non-linear model is linearized for testing assumptions of classical linear regression and the assumptions are confirmed for both models. First, the data of 2010 is modeled by regression to decide whether the useful model is linear or non-linear. The results of 2010 year model proved that linear models were the most appropriate model for geothermal power plants.
- Therefore, all annual regression models were parametrically developed as linear. The annual regression applications showed that serial autocorrelation was the most important problem during performance modeling of geothermal power plants. Therefore, autocorrelations were eliminated by Orcutt-Cochran method while regression models for the performance of the geothermal power plant were built for each year. According to annual regression models, performance status of the plant is variable from year to year. During the 2006-2008, the trends are similar. However, the plant performance has started to decrease with 270 kW_e electricity generation capacity since 2009. The total degradation of the plant performance increased with 760 kW_e capacity by 2012.

- **Comparison of the net power correction factors of theoretical and regression models with Ormat performance model**

  - The net power correction factors of DORA-1 GPP were given by Ormat. The theoretical and statistical net power correction factors are also calculated by using thermodynamic model and regression analysis of 2008 year, respectively.
  - Although there are some minor differences, all of the net power correction factors have similar trends. The statistical net power correction factors for regression model are slightly different than Ormat correction factors.
  - The comparison shows that, Ormat's correction factors don't exactly express the performance status of the DORA-1 GPP.

Consequently, the performance equations of a geothermal power plant are computerized by thermodynamic and regression analysis, and then they are compared with DORA-1 GPP's manufacturer performance equations. Furthermore, the degradation of plant performance of DORA-1 geothermal power plant is also found by regression.

REFERENCES

Amjady, N., Keynia, F., Zareipour, H., Short-term wind power forecasting using ridgelet neural network. Electric Power Systems Research 81 (2011) 2099-2107.

Aneke, M., Agnew, B. Underwood, C.: Performance analysis of the Chena binary geothermal power plant. *Appl. Therm. Eng.* 31 (2011), pp. 1825–1832.

Ben-Nakhi, A.E., Mahmoud., M.A., Cooing load prediction for buildings using general regression neural networks. Energy Conversion and Management 45 (2004) 2127-2141.

Breusch, T., S., Pagan, A., R., A Simple Test for Heteroscedasticity and Random Coefficient Variation. Econometrica, Vol. 47, 1287–1294, 1979.

Bronicki, L.: Innovative geothermal power plants, fifteen years experience. *Proceedings World Geothermal Conference*, Florence, Italy, 1995.

Carta, J.A., Velazquez, S., Matias, J.M., Use of Bayesian networks classifiers for long-term mean wind turbine energy output estimation at a potential wind energy conversion site. Energy Conversion and Management 52 (2011) 1137-1149.

Celik, H., M., CP-790 Statistical Modeling and Forecasting Course Notes, İzmir, 2011.

Cengel, Y.A., Boles, M.A., Thermodynamics: An engineering approach. 5th ed. McGraw-Hill.

Chamorro, C. R., Mondejar, M.E., Ramos, R., Sedovia, J.J, Martin, M.C., Villamanan, M.A., World geothermal power production status: Energy, environmental and economic study of high enthalpy technologies, Energy 42 (2012), pp. 10-18, 2012.

Cho, S-H., Kim, W-T., Tae, C-S., Zaheeruddin, M., Effect of length measurement period on accuracy of predicted annual heating energy consumption of buildings. Energy Conversion and Management 45 (2004) 2867-2878.

Chung, W., Using the fuzzy linear method to benchmark the energy efficiency of commercial buildings. Applied Energy 95 (2012) 45-49.

Cochrane, D., Orcutt, G., H., Application of least squares regression to relationships containing autocorrelated error terms. Journal of the American Statistical

Association, Vol. 44, 32–61, 1949.

Coskun, C., Oktay, Z., Dincer, I., Performance evaluations of a geothermal power plant',Applied Thermal Engineering 31 (2011),pp. 4074-4082

Danov, S., Carbonell, J., Cipriano, J., Marti-Herrero, J., Approaches to evaluate building energy performance from daily consumption data considering dynamic and solar gain effects. Energy and Buildings. DOI: 10.1016/j.enbuild.2012.10.050.

Dipippo, R., Second Law assessment of binary plants generating power from low-temperature geothermal fluids, Geothermics 33 (2004), pp. 565-586.

DiPippo, R.: *Geothermal power plants: principles, applications, case studies*. First Edition, Elsevier Advanced Technology, Oxford, 2005.

Dipippo, R., Ideal thermal efficiency for geothermal binary plants. Geothermics 36 (2007), pp. 276-285.

Drapper, N., R., Smith, H., Applied Regression Analysis. John Wiley & Sons, 1998, 3rd ed. New York.

Douak, F., Melgani, F., Benoudjit, N., Kernel ridge regression with active learning for wind speed prediction. Applied Energy Volume 103 (2013) pp. 328-340.

EES: Ver. 9.250:#2756: For use only in the Dept. of Mechanical Engineering. Izmir Institute of Technology, Izmir, Turkey, 2013.

EMRA, Republic of Turkey Energy Market Regulatory Authority. Retrieved June 06, 2013, from http://lisans.epdk.org.tr/epvys-web/faces/pages/lisans/elektrikUretim/elektrikUretimOzetSorgula.xhtml

Franco, A.: Power production from a moderate temperature geothermal resource with regenerative organic Rankine cycles. *Energy Sustain. Develop.* 15 (2011), pp. 411–419.

Freire, R., Z., Oliveria, G.H.C., Mendes, N., Development of regression equations for prediction energy and hygrothermal performance of buildings. Energy and Buildings 40 (2008) 810-820.

Fu, W., Zhu, J., Zhang, W., Lu, Z., Performance evaluation of Kalina cycle subsystem on geothermal power generation in the oilfield. Applied Thermal Engineering 54

(2013), pp. 497-506.

Ganjehsarabi, H., Gungor, A., Dincer, I., Exergetic performance analysis of Dora II geothermal power plant in Turkey. Energy 30 (2012), 1-8.

GEA (Geothermal Energy Association), Geothermal Basics: Q&A, September 2012.
E&GI: Energy and Geoscience Institute. Retrieved June 06, 2012 from http://geo-energy.org/reports/Gea-GeothermalBasicsQandA-Sept2012_final.pdf

GEO (Geothermal Education Office), Retrieved June 06, 2012 from http://geothermal.marin.org/GEOpresentation/sld050.htm

Ghani, I., M., Ahmad, S., Stepwise Multiple Regression Method to Forecast Fish Landing. Procedia Social and Behavioral Sciences 8 (2010) 549–554.

Ghasemi, H., Paci, M., Tizzanini, A., Mitsos, A., Modeling and optimization of a binary geothermal power plant. Energy 50 (2013), pp. 412-428.

Ghiaus, C., Experimantal estimation of building energy performance by robust regression. Energy and Buildings 38 (2006) 582-587.

Gokcen, G., Ozturk, H.K. & Hepbasli, A.: Overview of Kizildere geothermal power plant in Turkey. *Energy Convers. Manage.* 45 (2004), pp. 83–98.

Gujarati, D., N., Basic Econometrics. McGraw Hill, 2003, 4rt ed. The United States.

Gupta H.; Roy, S. Worldwide Status of Geothermal Resource Utilization, Geothermal Energy, Elsevier, ISBN-13: 978-0-444-52875-9, 2007, pp. 199-229.

Guo, T., Wang, H.X., Zhang, S.J., Fluids and parameters optimization for a novel cogeneration system driven by low-temperature geothermal sources. Energy 36 (2011), pp. 2639-2649.

Gülgezen, G., Sumer, E., C., Aytaç, S., Toksoy, M., GEOPERFORM programme for development of a database and performance monitoring in geothermal power plants, Proceedings Geothermal Energy Seminar - TESKON 2007, İzmir.

Hettiarachchi, H.D.M., Golubovic, M., Worek, W.M., Ikegami, Y., Optimum design criteria for an Organic Rankine cycle using low-temperature geothermal heat source. Energy 32 (2007), pp. 1698-1706.

Jobson, J., D., Applied Multivariate Data Analysis, Volume I: Regression and

Experimental Design. Springer-Verlag New York, 1999 (e-book: http://www.google.com.tr/books).

Kakaç, S., Liu, H., "Heat Exchangers: Selection, Rating and Thermal Designing", 2nd Ed., CRC Press, 2002.

Kaplan, U. & Serpen, U.: Developing geothermal power plants for geothermal fields in western Turkey. *Proceedings World Geothermal Congress 2010*, 25–29 April 2010, Bali, Indonesia, 2010.

Kanoglu, M.: Second Law Analysis of Geothermal Power Plants. Proceedings Geothermal Energy Seminar-TESKON 2007, İzmir.

Kanoglu, M., Exergy analysis of a dual-level binary geothermal power plant. Geothermics 31 (2002), pp. 709-724.

Kanoglu, M., Bolatturk, A., Performance and parametric investigation of a binary geothermal power plant by exergy. Renewable Energy 33 (2008), 2366-2374.

Katipamula, S., Reddy, T.A., Claridge, D.E., Bias in predicting annual energy use in commercial buildings with regression models developed from short data sets. ASME Solar Energy Conference Proceedings, November 1994.

Kaza, N., Understanding the spectrum of residential energy consumption: A quantile regression approach. Energy Policy 38 (2010) 6574-6585.

Lam, J.C., Hui, S.C.M., Chan, A.L.S., Regression analysis of high-rise fully air-conditioned office buildings. Energy and Buildings 26 (1997) 189-197.

Lam, J.C., Wan, K.K.W., Liu, D., Tsang, C.L., Multiple regression models for energy use in air-conditioned office buildings in different climates. Energy Conversion and Management 51 (2010) 2692-2697.

Lee, W-S., Evaluating and ranking energy performance of office buildings using fuzzy measure and fuzzy integral. Energy Conversion and Management 51 (2010) 197-203.

Liu, H., Shi, J., Qu, X., Empirical investigation on using wind speed volatility to estimate the operation probability and power output of wind turbines. Energy Conversion and Management 67 (2013) 8-17

MENR, The Ministry of Energy and Natural Resources: Energy Information about Ministry. Retrieved August 15, 2012, from http://www.enerji.gov.tr/index.php?dil=en&sf=webpages&b=elektrik_EN&bn=219&hn=&nm=40717&id=40732

Mines, G.L., Evaluation of theimpact of off-design operation on an air-cooled binary power plant. Geothermal Resource Council Annual Meeting (2002), INEEL/CON-02-00793.

O'Brien, R., M., A Caution Regarding Rules of Thumb for Variance Inflation Factor. Quality and Qantity, Vol. 41, 673-690, 2007.

Ormat, Aydın Salavatlı geothermal power plant, Operation and maintenance manual, 2004.

Ormat, Salavatlı geothermal project, final acceptance performance tests: general procedure, 2005.

Ozcan, N., Y., Modeling, simulation and optimization of flashed-steam geothermal power plants from the point of view of noncondensable gas removal systems. PhD Thesis in Mechanical Engineering, The Graduate School of Engineering and Sciences, Izmir Institute of Technology, Izmir, Turkey, June 2010.

Prais, S., J., Winsten, C., B., Trend Estimators and Serial Correlation. Cowles Commision Discussion Paper, Statistics No. 383., 1954.

Salcedo-Sanz, S., Ortiz-Garcia, E.G., Perez-Bellido, A.M., Portilla-Figueras, A., Short term wind speed prediction based on evolutionary support vector regression algorithms. Expert Systems with Applications 38 (2011) 4052-4057.

Shokouhmand, H. & Atashkadi, P.: Performance improvement of a single, flashing, binary, combined cycle for geothermal power plants. *Energy* 22:7 (1997), pp. 637–643.

Sonntag, R.E., Borgnakke, C., Van Wylen, G.J., Fundamentals of thermodynamics. 6th ed., John Wiley & Sons, Inc., 2002.

SPSS 17.0 Statistical Package for the Social Sciences Programme.

Swandaru, R.B.: Modeling and optimization of possible bottoming units for general

single-flash geothermal power plants. MSc thesis, Department of Mechanical and Industrial Engineering University of Iceland, Reykjavík, Iceland, 2009.

TGNA_1, Turkish Grand National Assembly, Law Number: 5084, Official Newspaper: 25365, 06.02.2004. Retrieved December 08, 2012, from http://www.sanayi.gov.tr/Files/Mevzuat/yatirimlarin_ve_istihdaml-13042010211153.pdf

TGNA_2, Turkish Grand National Assembly, Law Number: 6094, Official Newspaper: 27809, 08.01.2011. Retrieved December 08, 2012, from http://www.enver.org.tr/modules/mastop_publish/files/files_4ed5f2332448e.pdf

Tso, G.K.F., Yau, K.K.W, Predicting electricity energy consumption: A comparison of regression analysis, decision tree and neural netwoks. Energy 32 (2007) 1761-1768.

Utsunomiya, H., Nagao, F., Urakami, I., Regression analysis of local wind properties with local topographic factors. Journal of Wind Engineering and Industrial Aerodynamics 74-76 (1998) 175-187.

Valdimarsson, P., Production of electricity from geothermal heat-efficiency calcultion and ideal cycles. International Geothermal Conference, Reykjavik, Sept. 2003.

WWW_spsstools, 2012: Retrieved May 18, 2012, from http://www.spsstools.net/Syntax/RegressionRepeatedMeasure/Breusch-PaganAndKoenkerTest. txt